

Article

A Reconstruction of Irrigated Cropland Extent in China from 2000 to 2019 Using the Synergy of Statistics and Satellite-Based Datasets

Minghao Bai ^{1,2}, Shenbei Zhou ^{2,3,4,*}  and Ting Tang ⁵ ¹ College of Environmental Sciences and Engineering, Peking University, Beijing 100871, China² Water Resources Economics Research Institute, Hohai University, Nanjing 211100, China³ Business School, Hohai University, Nanjing 211100, China⁴ Global Environment and Natural Resources Institute (GENRI), College of Science, George Mason University, Fairfax, VA 22030, USA⁵ International Institute for Applied Systems Analysis (IIASA), A-2361 Laxenburg, Austria

* Correspondence: shenbei@hhu.edu.cn

Abstract: Irrigated agriculture has undergone rapid developments in China, which has greatly increased food production but overexploited water resources as well. Spatial information on irrigated cropland is critical to balance irrigation yield gains against the negative impact on water resources. However, remote-sensing-based maps on irrigated areas with short temporal coverage often suffer from undermined accuracy in humid areas and inconsistency with statistics, which limit their applications in food policy and water management. The following study integrates existing irrigation maps, observed data on irrigated cropping system, and statistics by a synergy approach to map irrigated areas in China from 2000 to 2019. We also incorporate past information on actual irrigation to avoid divergence between observations and statistics from its fluctuation. Afterwards, 614 reference samples across mainland China have been used to validate resultant maps, which show that outperformance was above overall accuracy and Kappa coefficients. Moreover, our maps share a similar spatial pattern with Irrimap-Syn maps rather than remote-sensing-based maps (CCI-LC). Irrigated areas have grown rapidly from 55.42 Mha in 2000 to 71.33 Mha in 2019 but with different growth trends in different regions. Simultaneous large-scale expansion and abandonment occur in the Huang-Huai-Hai Plain and Yangtze River Basin, while the Northwest Inland Region and the Northeast Plain are the two largest net area gains. Rainfed croplands are dominant sources of expansion, followed by pastures, respectively, with over 70% and 20% contributions in total gains. This not only is a shift from rainfed to irrigated systems but also indicates an intensification of agriculture, which might contribute to agricultural drought reductions in the north and wide soil suitability. Other efforts on agricultural sustainability also have been detected, such as geographical shifts from vulnerable to relatively suitable areas, grain for green, cropland protection, and cropland protection in the competition of urbanization.

Keywords: irrigated cropland dynamics; synergy mapping approach; land-use transition; China



Citation: Bai, M.; Zhou, S.; Tang, T. A Reconstruction of Irrigated Cropland Extent in China from 2000 to 2019 Using the Synergy of Statistics and Satellite-Based Datasets. *Land* **2022**, *11*, 1686. <https://doi.org/10.3390/land11101686>

Academic Editors: Tesfay Gebretsadkan Gebremicael, Ermias Teferi and Woldeamlak Bewket

Received: 28 August 2022

Accepted: 26 September 2022

Published: 29 September 2022

Publisher's Note: MDPI stays neutral with regard to jurisdictional claims in published maps and institutional affiliations.



Copyright: © 2022 by the authors. Licensee MDPI, Basel, Switzerland. This article is an open access article distributed under the terms and conditions of the Creative Commons Attribution (CC BY) license (<https://creativecommons.org/licenses/by/4.0/>).

1. Introduction

Agricultural land, covering about 37.6% of the Earth's land surface, is withstanding increasing food demand at an unprecedented rate with continuous population and consumption growth [1–5]. Irrigation plays a significant role in feeding the growing population by enhancing grain yields [6–14]. However, as the dominant water user, irrigated withdrawal accounts for about 60% of available freshwater, leading to reductions in streamflow and groundwater recession [15–18]. Thus, global food production is constrained by the local availability of freshwater [17,19,20]. With food demand growth, long-term water shortage, intense land competition, and climate change, future increasing tensions between

food and water securities are expected [21–25]. As a large food demand country limited by the uneven distribution of water resources and insufficient arable land per capita, China relies heavily on irrigation for grain production, which has contributed three-quarters of the total in 2019 [26–30]. The expansion of irrigated cropland is driven by large-scale water conservancy construction, which helps mitigate grain losses caused by floods and droughts [31,32]. Meanwhile, China's water policies are also heavily tied to water conservancy projects [33]. It is critical to balance irrigation's yield gains against the negative impact on water resources, which is still constrained by a lack of explicit and accurate information on where irrigated land distributes and how it develops [13,24,34–39]. Therefore, quantifying and understanding spatial changes in irrigated cropland and its temporal dynamics are vital foundations for monitoring food and water securities.

Mapping irrigated areas is performed either by using agricultural censuses or using remote sensing data [40]. Statistics often provide highly suitable land-use information with respect to long-term periods, but they are bound to administrative units, thus lacking spatial details [38,41,42]. As an advanced tool, satellite remote sensing has been widely used to monitor land cover and land use at high spatial resolutions but it has short temporal coverage [35,42,43]. Many studies have made efforts to map irrigated cropland from local to global scales, but they seldom can show the entire picture of China. These maps include global irrigation areas (GIA) at 30 arcsec resolutions based on Global Map of Irrigation Areas version 5 (GMIAv5) [19]; a Global Rain-Fed, Irrigated, and Paddy Cropland (GRIPC) map circa 2005 at 500 m resolution [44]; a global irrigated and rainfed cropland extent map at nominal 1 km circa 2010 provided by Global Food Security-Support Analysis Data (GFSAD) [45]; Irrigated Area Map for Asia and Africa (IAAA) at 250 m resolution; a 1 km irrigated area map in China (CIM) in 2000 [32]; and an irrigated area map for China in 2016 with a resolution of 500 m (Xiang's map) [46], etc. Several efforts also have been made with respect to long-term temporal coverage, such as the Climate Change Initiative Land Cover (CCI-LC) produced by the European Space Agency (ESA) [47], the historical irrigated cropland distribution derived from the History Database of the Global Environment (HYDE) [48], and a new dataset of global irrigation areas from 2001 to 2015 (NGIA) [24]. However, they often suffer from undermined accuracy in humid areas because of similar signals between irrigated and rainfed croplands [32,49,50]. More importantly, their estimated areas are often not consistent with statistics, which limits their applications in food policy and water management [41,51].

Generally, each data source on its own is unable to capture the full scale of land use dynamics due to the absence of key components, such as space and time [42]. Data synergy approaches provide a feasible way to solve this by integrating all available remote sensing datasets and statistics to take advantage of their complementarities [8,34,41]. For example, Fritz et al. (2015) integrated several individual cropland maps from global to regional scale to develop a new global cropland percentage map circa 2005 [52]. Lu et al. (2017) developed a hybrid cropland map of China in 2010 by fusing five existing cropland products and sub-national statistics [53]. In terms of irrigated croplands, a recent study combines remote sensing datasets with statistics by an agreement method to map annual synergy irrigation areas (IrriMap_Syn) from 2000 to 2019 [14]. It directly equates the current year's remote sensing data to statistics, but it may ignore their differences in areas, which refer to the actual irrigated area (AAI) and area equipped irrigation (AEI) [32,34]. AAI often is lower than AEI, when no irrigation occurs in irrigated croplands, such as land fallow and rotation from irrigated to rainfed crops [54]. In order to reduce the gap between AEI and AAI and spatio-temporal fluctuations caused by actual irrigation or cropping behaviors, AEI is estimated not only by the observed area of the current year but also by incorporating past areas of actual irrigation [54,55].

Our research objectives are to map irrigated cropland distributions that are consistent with statistics in mainland China from 2000 to 2019 by using the synergy of multiple heterogeneous data streams and to further track irrigated cropland changes and their impacts on agricultural development based on our resultant maps. To achieve these

objectives, we firstly integrate existing irrigation maps, observed data on irrigated cropping system, and statistics by using an agreement-scoring method to develop irrigated cropland extents at 30 arcsec resolution (~ 1 km at equator) in mainland China from 2000 to 2019. Second, we apply 614 reference samples to validate resultant maps and analyze spatial patterns and changing trends with respect to irrigated croplands by comparing other time-series datasets. Finally, we, using resultant maps, track spatio-temporal changes with respect to irrigated croplands and analyze their impacts on agricultural development based on land-use transitions. These generated maps provide explicit and accurate information on where irrigated lands are distributed and how the distribution is developed at a national scale for the last twenty years, which enable scientists and policymakers in better addressing food security, water resources management, and land-use planning with respect to the sustainable development of irrigated agriculture.

2. Data and Methods

2.1. Study Area

The study area encompassed 7 geographical units in mainland China, with a total of 31 provincial-level administrative units, such as Beijing, Tianjin, and Hebei, etc., excluding Hong Kong, Macao, and Taiwan, as shown in Figure 1.

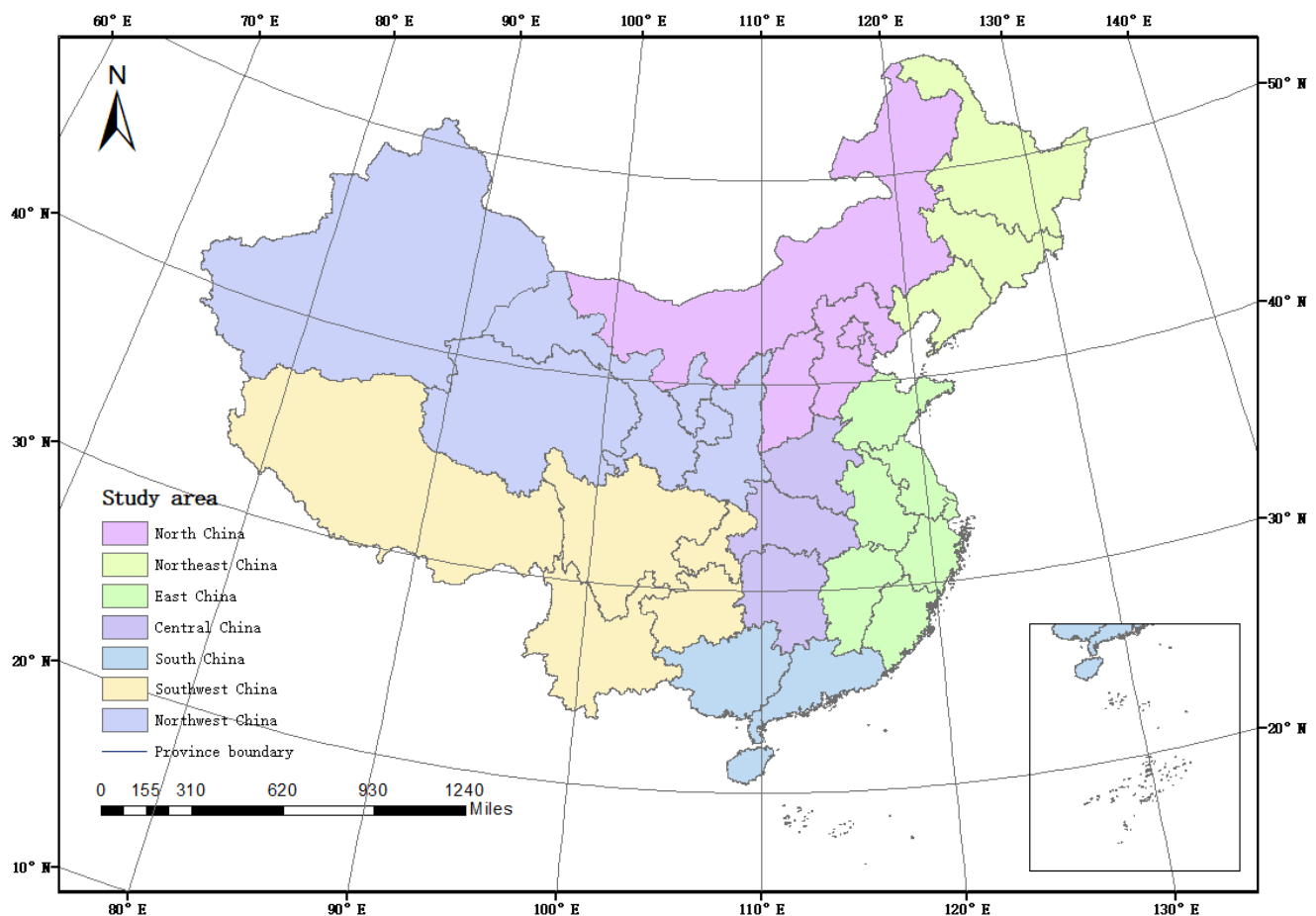


Figure 1. The study area.

2.2. Input Data

2.2.1. Cropland Extent Data

The data used in this study included global- and local-gridded products on cropland and irrigation at different spatio-temporal resolutions and provincial-level statistics for irrigated cropland areas, as shown in Table 1. At first, all gridded data were resampled to

30 arcsec resolution ($\sim 1 \text{ km}^2$ at the Equator) with WGS84 datum, for which its size is close to that of large fields or the agglomeration of smaller irrigated field [19]. However, limited by cropland fragmentation and the small-scale economics of rural households, the field size might be much smaller than 1 km^2 in China [52]. To reduce the overestimation caused by the difference between pixel size and actual field size, we introduced cropland coverage within pixels. The applied cropland coverage was combined by three land cover (LC) datasets, including HHistoric Land Dynamics Assessment+ (HILDA+) [56], Climate Change Initiative Land Cover (CCI-LC) [47], and China's Land-Use/cover Dataset (CLUD) [57].

Table 1. Applied satellite-based products.

No.	Type	Name	Spatial Resolution	Temporal Resolution	Applied Data
1	LULC	CCI_LC	300 m, Global	Annual, 1992–2019	(Irrigated) cropland
2		CLUD	1 km, China	5-year, 1980–2020	Cropland
3		HILDA+	1 km, Global	Annual, 1980–2019	Cropland
4	Existing irrigation maps	CIM	1 km, China	Annual, 2000	Irrigated cropland
5		GIA	30 arcsec, Global	Annual, 2005	Irrigated cropland
6		GRIPC	500 m, Global	Annual, 2005	Irrigated cropland
7		IAAA	250 m, Asia	Annual, 2000 & 2010	Irrigated cropland
8		GFSAD	1 km, Global	Annual, 2010	Irrigated cropland
9		Xiang2016	500 m, China	Annual, 2016	Irrigated cropland
10		GLC_FCS	30 m, China	5-year, 2015–2020	Irrigated cropland
11	Cropping system data	ACIA	500 m, Asia	Annual, 2001–2019	Actual CI
12		APRA	500 m, Asia	Annual, 2000–2019	Paddy rice
13		ChinaCropArea 1 km	1 km, China	Annual, 2000–2015	Wheat
14		GAEZ	5 arcmin, global	Static, 1981–2010	Potential rainfed CI

HILDA+ (Historic Land Dynamics Assessment + dataset) provided six well-defined land-cover categories (cropland, urban, pasture, forest, unmanaged grass/shrubland, and sparse) to quantify annual dynamics of global land use change from 1960 to 2019 at a spatial resolution of 1 km [42,56]. It was more persuasive than a single dataset, since it was built on multiple heterogeneous data streams (remote sensing, reconstructions, and statistical data) [42], but its spatial resolution could not meet the requirement of field size. Thus, we further introduced cropland coverage with higher spatial resolutions (300 m) from CCI-LC, which also was the input data of HILDA+. Thus, these two datasets could retain high spatial consistency. Moreover, CCI-LC had high accuracies in rainfed and irrigated croplands at 0.85 and 0.88, respectively [47]. To strengthen the reliability, we also introduced a local dataset (CLUD), which was generated by a visual interpretation of Landsat and CBERS imagery with high overall accuracies for all class levels [57]. Among them, HILDA+ was used as the core LC input. The upper limitations of cropland coverage for 1 and 0.4 km^2 in grids of cropland and non-cropland were set in accordance with cropland definitions in HILDA+ [42,56]. The cropland coverage obtained from other two datasets was introduced, and the largest and smallest coverages were obtained in cropland pixels. In the subsequent allocation of irrigated areas, we preferentially allocated the smallest coverage, followed by an area difference between the largest and smallest areas if the smallest area was not enough.

2.2.2. Statistical Area of Irrigated Cropland

According to the definition of cropland in HILDA+, we collected the statistical irrigation area of cultivated land and orchard at the provincial level from the *China Agriculture Statistical Report* (1949–2019) and *China Water Statistical Yearbooks* from 2000 to 2019. These statistics can be accessed from the Statistical Database of Economic and Social Development by the National Knowledge Infrastructure of China (<https://data.cnki.net/HomeNew/Index>, last access: 20 July 2022).

2.2.3. Existing Irrigation Maps

Existing irrigation maps were obtained from two sources: irrigated cropland from LC data and independent irrigation maps. GLC_FCS also provided irrigated cropland data in 2015 and 2020, which were developed by local trained random forest models with time-series Landsat imageries [58]. Several global and regional irrigation maps were also applied as inputs, including CIM, IAAA, GRIPC, GMIA-m, GFSAD (global food security-support analysis data), and Xiang2016. CIM is a 1 km irrigated cropland map around year 2000 by using a potential irrigation index to downscale census data [32]. IAAA, obtained from the International Water Management Institute (IWMI), was available at 250 m resolution for 2000 and 2010 to map irrigated and rainfed croplands in Asian and African regions [59]. GRIPC is a 500 m Global Rain-Fed, Irrigated, and Paddy Cropland map circa 2005, which was generated by supervised classifications with remote sensing, climate, and agricultural inventory data [44]. GMIA-m is a downscaled GMIAv5 map at 30 arcsec resolution [19]. GFSAD is generated by NASA and USGS to provide global cropland data for global food security [45]. Xiang 2016 is an irrigated area map for mainland China in 2016 at 500 m resolution by comparing the land surface water index with a normalized difference vegetation index [46].

2.2.4. Remote Sensing Data on Irrigated Cropping Systems

With the exception of existing irrigation maps, the distribution of irrigated fields can also be obtained from cropping systems. The difference between irrigated and rainfed cropping systems is explicit, which can provide accurate information on irrigated fields with high confidence. Two irrigated crop (rice and wheat) distributions were used as alternatives to irrigation extent. Rice is a dominant grain crop and is widely cultivated in south and northeast of China [60,61]. It is cultivated in paddy fields that are unsuitable for dryland crops and is considered as part of irrigated croplands with high confidence [36,60]. In its cultivation, irrigation is used not only to relieve crop drought stress but also to control water levels and suppress weed growth [54]. A 500 m annual paddy rice dataset (APRA) was applied in this study, providing a 500 m-grid of paddy rice maps of monsoon Asia (some countries) from 2000 to 2020 with an overall accuracy of 75% [62,63]. Wheat is also another main grain crop in China and is mainly produced in north with less precipitation during the growth period; thus, irrigation is required [64]. We obtained wheat distributions with 1 km resolution from a dataset of annual harvesting areas (ChinaCropArea1 km), which provided a 1 km-grid crop harvesting area dataset for three main crops of China from 2000 to 2015 [65]. Wheat classification had a high accuracy with R^2 values that were consistent around 0.85, under the county-level statistical data comparison [66].

Evidence was obtained from cropping intensities in distinguishing irrigated and rainfed fields, since there might be more crop cycles in irrigated conditions with the lifting of water-supply restrictions [67,68]. The potential cropping intensity gap between irrigated and rainfed scenarios in China increased due to increasing rainfed water-supply limitations from climate change since 1960s [67]. Thus, the difference between actual intensity and potential rainfed cropping intensity was used to determine whether irrigation was performed or not. Actual data were obtained from a 500 m annual cropping intensity dataset (ACIA), which provided annual maps covering monsoon Asia (some countries) from 2001 to 2020 [69]. The potential rainfed cropping intensity comprised static data from 1980 to 2010, which was taken from the GAEZv4 dataset [70].

2.3. Methods

2.3.1. Synergy Irrigation Mapping

The basic idea of the synergistic approach used in this study was to extract likely irrigated areas based on spatial agreements of multiple heterogeneous high spatial-resolution data and then to sum them within a specific administrative boundary to match statistical areas [36,41]. Three main components were involved in the synergy process, including all

possible irrigated pixel extraction within a specific temporal duration, agreement-ranking establishment, and statistical area allocation, as shown in Figure 2.

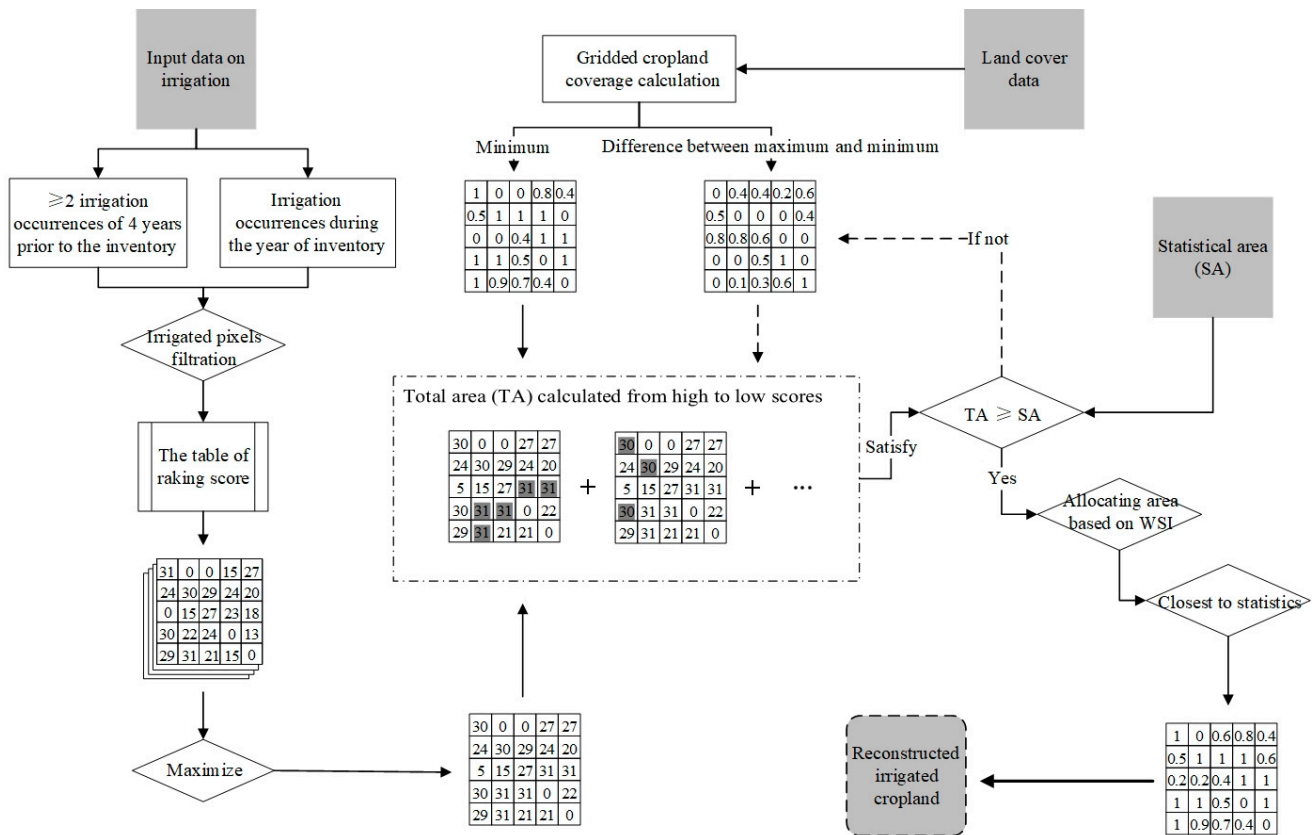


Figure 2. The scheme used for developing annual irrigation maps for mainland China.

Not all irrigated croplands can be detected by remote sensing during the year of inventory, because some irrigation infrastructures might not be in use, such as land fallow and crop rotation [54], resulting in a lower number of areas estimated from satellite-based datasets than area-equipped irrigation reported in the census dataset [54]. Therefore, we could not infer the location of all irrigated cropland from irrigation pixels of the current year alone derived from satellite-based data. In addition to irrigated areas during the year of inventory, a common method based on satellite-based data also incorporates areas where irrigation occurs during ≥ 2 of 4 years before the inventory [54,55]. Following this method, we collected all irrigation pixels, which met requirements for the past four years and the current year from time-series remote-sensing-based data (CCI-LC and cropping system data) to map the potential distribution of irrigated cropland during the year of statistics.

Integrating input data was performed by ranking rather than unequal weighting [52]. A suitable weight order of inputs was crucial for synergistic mappings because inputted accuracy assessments affected synergistic confidence [36,52,53]. Fritz et al. (2015) compared input products with crowdsourced data from Geo-Wiki to rank individual cropland products [52]. Lu et al. (2017) ranked existing cropland datasets using accuracy assessment based on sampling data [53]. Lu et al. (2020) also used the difference between the area derived from inputs and statistical area to assess their accuracy [41]. In addition, Zhang et al. (2022) used accuracy provided by input products themselves and expert-judgment-fused methods to rank the weight order [36]. Here, we set the weight order according to the following rules. At first, we took time-series datasets as the priority since they had higher time sensitivities in irrigated land distributions. Then, we used 614 validation samples described in Section 2.2 to assess the overall accuracies of input data. Datasets with outperformed accuracy assessments were ranked higher in the weight order. With respect

to slight differences in the overall accuracy, we further compared the differences between inputs and statistics and placed the data with smaller gaps in a higher order. Moreover, we grouped all input datasets into five groups for each year and labelled them A, B, C, D, and E from high to low rankings, as shown in Table 2. Due to the significant regional characteristics of cropping system distributions, which prevented them from covering most areas, we combined the data on wheat and irrigated cropping intensities with similar spatial patterns into group B, while rice was separately listed as group C.

Table 2. Input data applied for each year.

Year	A	B	C	D	E
2000	CCI-LC	Wheat	APRA	CIM	IAAA2000
2001	CCI-LC	Wheat & ACIA	APRA	CIM	IAAA2000
2002	CCI-LC	Wheat & ACIA	APRA	CIM	IAAA2000
2003	CCI-LC	Wheat & ACIA	APRA	GRIPC	GMIA-m
2004	CCI-LC	Wheat & ACIA	APRA	GRIPC	GMIA-m
2005	CCI-LC	Wheat & ACIA	APRA	GRIPC	GMIA-m
2006	CCI-LC	Wheat & ACIA	APRA	GRIPC	GMIA-m
2007	CCI-LC	Wheat & ACIA	APRA	GRIPC	GMIA-m
2008	CCI-LC	Wheat & ACIA	APRA	GFSAD	IAAA2010
2009	CCI-LC	Wheat & ACIA	APRA	GFSAD	IAAA2010
2010	CCI-LC	Wheat & ACIA	APRA	GFSAD	IAAA2010
2011	CCI-LC	Wheat & ACIA	APRA	GFSAD	IAAA2010
2012	CCI-LC	Wheat & ACIA	APRA	GFSAD	IAAA2010
2013	CCI-LC	Wheat & ACIA	APRA	Xiang 2016	GLC_FCS2015
2014	CCI-LC	Wheat & ACIA	APRA	Xiang 2016	GLC_FCS2015
2015	CCI-LC	Wheat & ACIA	APRA	Xiang 2016	GLC_FCS2015
2016	CCI-LC	ACIA	APRA	Xiang 2016	GLC_FCS2015
2017	CCI-LC	ACIA	APRA	Xiang 2016	GLC_FCS2015
2018	CCI-LC	ACIA	APRA	Xiang 2016	GLC_FCS2020
2019	CCI-LC	ACIA	APRA	Xiang 2016	GLC_FCS2020

CCI-LC: irrigated cropland distribution derived from Climate Change Initiative Land Cover; Wheat: wheat harvest distribution derived from China Crop Area1 km dataset; ACIA: a 500 m annual cropping intensity dataset; APRA: a 500 m annual paddy rice dataset; CIM: a 1 km irrigated area map in mainland China in 2000; GRIPC: a Global Rain-Fed, Irrigated, and Paddy Croplands map circa 2005; GFSAD: a global irrigated cropland extent map circa 2010 derived from global food security-support analysis data; Xiang2016: an irrigated area map for mainland China in 2016; IAAA 2000 and 2010: Irrigated Area Map for Asia and Africa (IAAA) at 250 m resolution circa 2000 and 2010; GMIA-m: a downscaled GMIAv5 map at 30 arcsec resolution derived from global irrigated areas dataset; GLC_FCS2015 and 2020: irrigated cropland distribution derived from global land-cover products with a fine classification system at 30 m in 2015 and 2020.

On this basis, an agreement ranking was built to reflect weight orders and agreement scores of the used inputs, as shown in Table 3. Agreement levels represented the spatial consensus among input layers as the number of input layers identifying a pixel as irrigated cropland. According to their spatial consensus and weight orders, the scores ranging from 0 to 31 represented the likelihood of irrigated cropland in pixels. Thus, the scoring table was used to transform heterogeneous input layers into an agreement-ranking map [41]. According to Tables 2 and 3, we used the year 2010 as the benchmark to present distributions of agreement levels and scores in Figure 3.

Table 3. The ranking scoring table for five groups of input data.

Agreement Level	Score	A	B	C	D	E
5	31	1	1	1	1	1
4	30	1	1	1	1	0
	29	1	1	1	0	1
	28	1	1	0	1	1
	27	1	0	1	1	1
	26	0	1	1	1	1

Table 3. *Cont.*

Agreement Level	Score	A	B	C	D	E
3	25	1	1	1	0	0
	24	1	1	0	1	0
	23	1	0	1	1	0
	22	1	1	0	0	1
	21	1	0	1	0	1
	20	0	1	1	1	0
	19	0	1	1	0	1
	18	1	0	0	1	1
	17	0	1	0	1	1
16	0	0	0	1	1	
2	15	1	1	0	0	0
	14	1	0	1	0	0
	13	1	0	0	1	0
	12	0	1	1	0	0
	11	1	0	0	0	1
	10	0	1	0	1	0
	9	0	1	0	0	1
	8	0	0	1	1	0
	7	0	0	1	0	1
	6	0	0	0	1	1
1	5	1	0	0	0	0
	4	0	1	0	0	0
	3	0	0	1	0	0
	2	0	0	0	1	0
	1	0	0	0	0	1
0	0	0	0	0	0	0

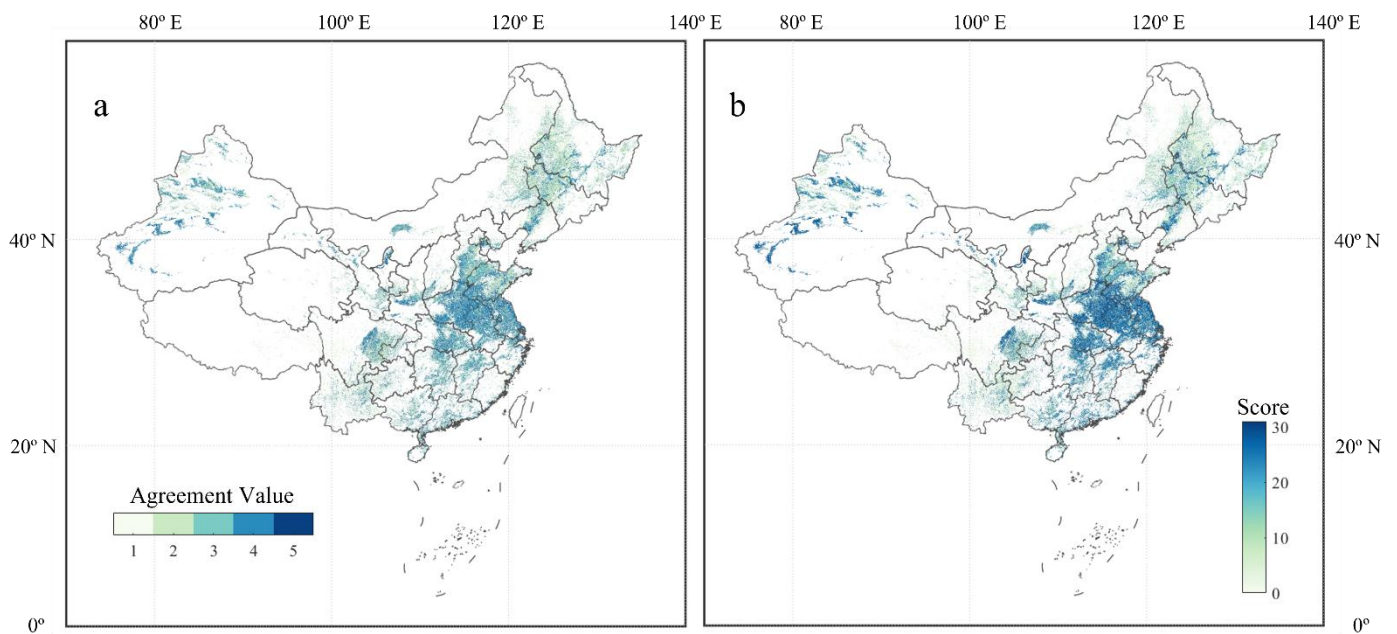


Figure 3. The spatial agreement levels (a) and scores (b) based on five groups of input data. The benchmark year is 2010.

Then, we allocated irrigated areas to the pixels in the order of largest to smallest scores until the cumulative gridded area within all specific administrative boundaries was close to the statistics. Thus, the irrigated area in each sub-national unit was allocated as follows:

$$Area_{i,s} = \sum_{s=31} p_{i,s} \times a_{m,y}, \quad (1)$$

where $Area_{i,s}$ denotes the cumulative irrigated area from score 31 to s in sub-national unit i , and $p_{i,s}$ denotes the pixel labeled as the cropland with agreement score s . $a_{m,y}$ represents the allocating cropland area in this pixel. The minimum cropland area of pixels was first allocated. If the minimum area was not sufficient for the requirement, we further allocated the differential area between the minimum and maximum areas.

To match statistical areas the statistical area ($Area_{i,Stat}$) was larger than $Area_{i,s-1}$ but smaller than $Area_{i,s}$, pixels with score s were further sorted according to agricultural drought. Because it was assumed that areas with more agricultural drought would be given priority for irrigation, agricultural drought was defined as the lack of soil to fulfil crop demands, which could be described by the evapotranspiration deficit index (ETDI) [71,72]. Due to the lack of monthly data on actual evaporation, we applied a simple crop water stress index (WS [0,1]) based on the annual evapotranspiration deficit, which was calculated by using potential and actual evaporation, as shown in Equation (2):

$$WS = \frac{PET - AET}{PET}, \quad (2)$$

where PET and AET represent the reference potential evaporation and actual evaporation covering a long-term period from 1981 to 2010, which were obtained from the GAEZv4 dataset [70]. A smaller WS represented a higher likelihood of irrigation due to long-term droughts in the area.

According to the WS index, we sorted pixels with agreement score s . Then, cropland areas of these pixels were allocated in order until statistical areas were matched, as shown in Equation (3):

$$Area_{i,Stat} \approx Area_{i,s-1} + \sum_{ws} p_{i,s}^{ws} \times a_{m,y}, \quad (3)$$

where $Area_{i,Stat}$ denotes the statistical area, which is larger than $Area_{i,s-1}$ but smaller than $Area_{i,s}$; $p_{i,s}^{ws}$ denotes the pixel with agreement score s and water stress index. In the end, annual synergic maps were generated from the resultant allocation.

2.3.2. Validation of Resultant Maps

To evaluate the overall accuracy of the resulting maps, 262 irrigated and 352 non-irrigated validation samples in mainland China were collected from Xiufang et al. (2014) [32], as shown in Figure 4. These samples were obtained from two sources, China Meteorological Data Sharing Service System (CMDSSS) and China Irrigation and Drainage Development Center (CIDDC). The former provided 352 non-irrigated and 156 irrigated samples but a lack of irrigated samples in the southeast, so another 106 irrigated samples were selected from 443 large irrigation districts provided by the latter (CIDDC). However, unlike CMDSSS, CIDDC provided general locations rather than geographical coordinates. Thus, these 106 samples were relocated by Google Earth, and farmlands near water sources were labelled as irrigated sites. More importantly, samples obtained from CMDSSS and CIDDC were suitable for validation because of large-scale spatio-temporal coverage. More detailed information of these samples can be observed in Xiufang et al. (2014) [32].

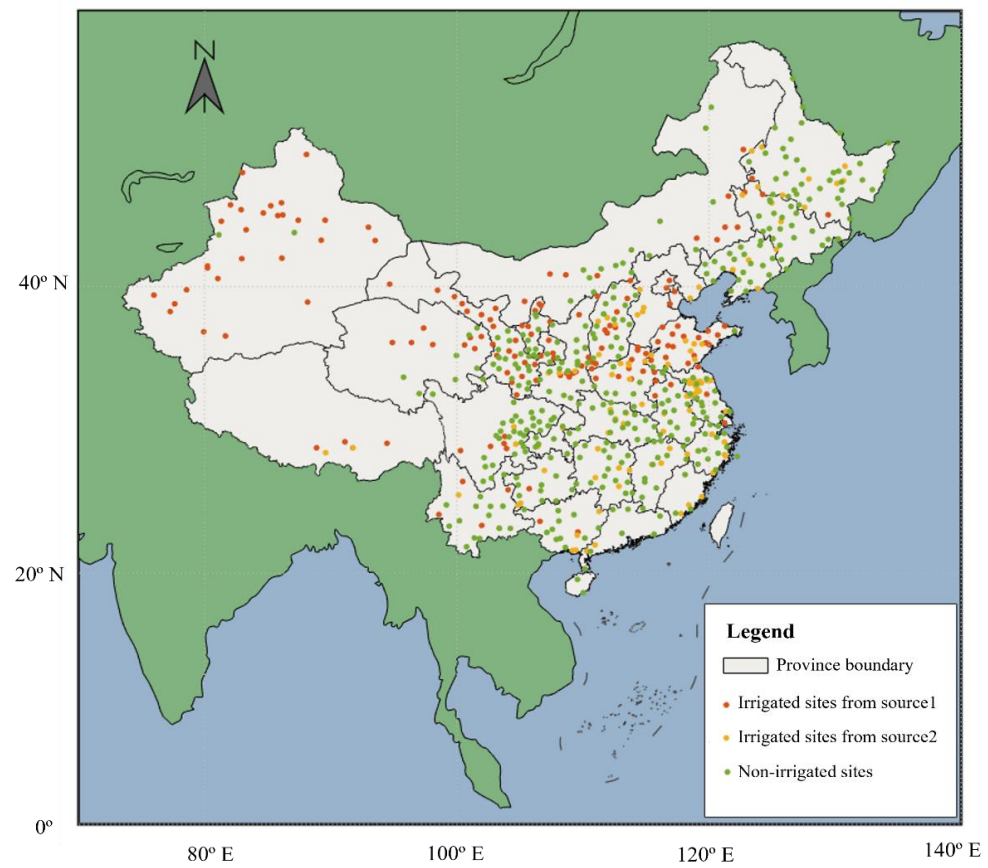


Figure 4. The distribution of validation samples in mainland China.

3. Results

3.1. Accuracy Assessment of the Rebuilt Dataset

We, using 614 validation samples (Figure 4), estimated the overall accuracy and Kappa coefficient of resultant maps and made comparisons with two time series (Irrimap-Syn and CCI-LC) and eight annual maps (group D and E of inputs) at the same spatial resolution (30 arcsec), as illustrated in Table 4. During 2000–2019, our average accuracy reached 69.54%, with the lowest and highest accuracies being 65.96% in 2000 and 71.66% in 2017 (Table 4), and accuracies in other years all fluctuated slightly around the average except for year 2000. The lowest accuracy is more of an anomaly due to insufficient input data in 2000, and it demonstrated that adequate input data could improve the accuracy of synthetic irrigation map. Interestingly, the increase in irrigated area did not necessarily lead to an improvement in overall accuracy. The accuracy circa 2005 should reach around 70%, but it decreased to less than 69% circa 2010 (Table 4). This phenomenon also occurred in Irrimap-Syn where the dropping accuracy lasted from 2000 to 2013. Here, it might share a close relation to input data accuracy, as far as the accuracy of input data (GRIPC and GMIA-m) in 2005 was higher than that (GFSAD and IAAA2010) in 2010 (Table 4). Although the accuracy of input data (Xiang’s map and GLC_FCS) in 2015 was still lower (Table 4), the increase in irrigated area may compensate for the classification gap of input data.

Overall, the accuracy of the reconstructed dataset was improved from using input data, the outperforming time series (CCI-LC), and annual (group D) datasets at an average of 3.58% and 4.48% higher. In comparison with the third-party data (Irrimap-Syn), it still maintained a 1.62% advantage in average accuracy. These accuracy estimates were also credible since accuracies of CIM and Xiang’s map were similar to the results of Xiang et al. (2016) [46]. The Kappa coefficient further supported the accuracy of our classification, and its values were higher than others in different years and average levels.

Table 4. The accuracy assessment of this study and comparison with other datasets.

		Time-Series Dataset			Annual Dataset	
		This Study	Irrimap-Syn	CCI-LC	Group D	Group E
2000	Correctly classified pixels	405	423	395	390	321
	Overall accuracy	65.96%	68.89%	64.33%	63.52%	52.28%
	Kappa coefficient	0.28	0.34	0.26	0.23	0.11
2005	Correctly classified pixels	433	415	401	416	404
	Overall accuracy	70.52%	67.59%	65.31%	67.75%	65.80%
	Kappa coefficient	0.37	0.31	0.28	0.34	0.24
2010	Correctly classified pixels	423	413	410	386	315
	Overall accuracy	68.89%	67.26%	66.78%	62.87%	51.30%
	Kappa coefficient	0.34	0.3	0.31	0.19	0.08
2015	Correctly classified pixels	425	424	407	384	298
	Overall accuracy	69.22%	69.06%	66.29%	62.54%	48.53%
	Kappa coefficient	0.34	0.34	0.3	0.19	0.08
Mean	Correctly classified pixels	427	417	405	\	\
	Overall accuracy	69.54%	67.92%	65.96%	\	\
	Kappa coefficient	0.35	0.32	0.29	\	\

3.2. Spatial Pattern Comparison among the Rebuilt Dataset with Other Existing Datasets

The irrigated cropland area in mainland China grew from 55.42 to 71.33 Mha over the last two decades (Figure 5a), which has profoundly changed the spatial pattern of irrigation distributions. However, not all existing irrigation datasets have realized the substantial change. Figure 5a highlighted differences in the gross irrigated area and the overall trend derived from statistics and gridded irrigation datasets, including most input datasets (except for some overestimated or underestimated data such as GFSAD and IAAA) and another three time-series datasets (Irrimap-Syn, HYDE, and NGIA). Our rebuilt time-series irrigation extent was obviously consistent with respect to the magnitude and overall trend of reported national irrigated areas (Figure 5a), while the other four time-series datasets showed significant discrepancies with statistics in the magnitude or overall trend (Figure 5a).

At first, NGIA predicted the subsequent irrigation distribution based on existing irrigation distribution in the past but ignored the subsequent irrigation expansion, so its estimated gross area would not exceed the maximum value in the past. Secondly, HYDE was a mapping of AAI, so it was acceptable that AAI was smaller than AEI. The divergence was not limited to differences between AEI and AAI. As directly evidenced, irrigated areas in some regions, such as Shandong Province, Henan Province, and Jiangsu Province, were illogically greater than AEI derived from statistics (Table A1). Thirdly, the irrigation distribution of CCI-LC was generated by a remote-sensing-based approach. However, its classification was often limited by many factors, such as humid environment, fertilizer use, plant protection, soil properties, and the change in crop-rotation system, etc. [32,49,50,73]. Similarly, annual maps such as GRIPC, IAAA, Xiang's Map and GLC_FCS, also showed great differences in classification accuracy and variances in area estimation (Table 4 and Figure 5a). Although CCI-LC had a relative advantage in classification accuracy, there was still a huge gap between the estimated area and the statistical one. Another reasonable guess was that it used a fixed set of ground samples in a specific period for a relatively stable area estimation.

Irrimap-Syn, as a dataset generated by statistics, showed a similar increasing overall trend, but it surprisingly had a magnitude gap with statistics, which increased from 2.95 Mha in 2000 to 5.85 Mha in 2019 (Figure 5a). As a reference, CIM and GMIA-m also showed gaps in statistics in the gross area, which could be explained by the exclusion of the irrigated orchard area (1.60 Mha) and the inclusion of irrigated areas in other land covers (5.01 Mha), respectively. However, this explanation did not apply to Irrimap-Syn,

because the average difference was still around 2 Mha, even excluding the irrigated area of the orchard. One possible reason for this discrepancy was that some statistical data at municipal and county levels were not available [36]. Such underestimation not only affected spatial pattern of irrigated cropland but also might have led to a difference in growth amplitude or trend (Figure 5b and Table A1). Overall, our resultant maps were more consistent with statistics than Irrimap-Syn, which avoided spatio-temporal discrepancies caused by gaps in statistics.

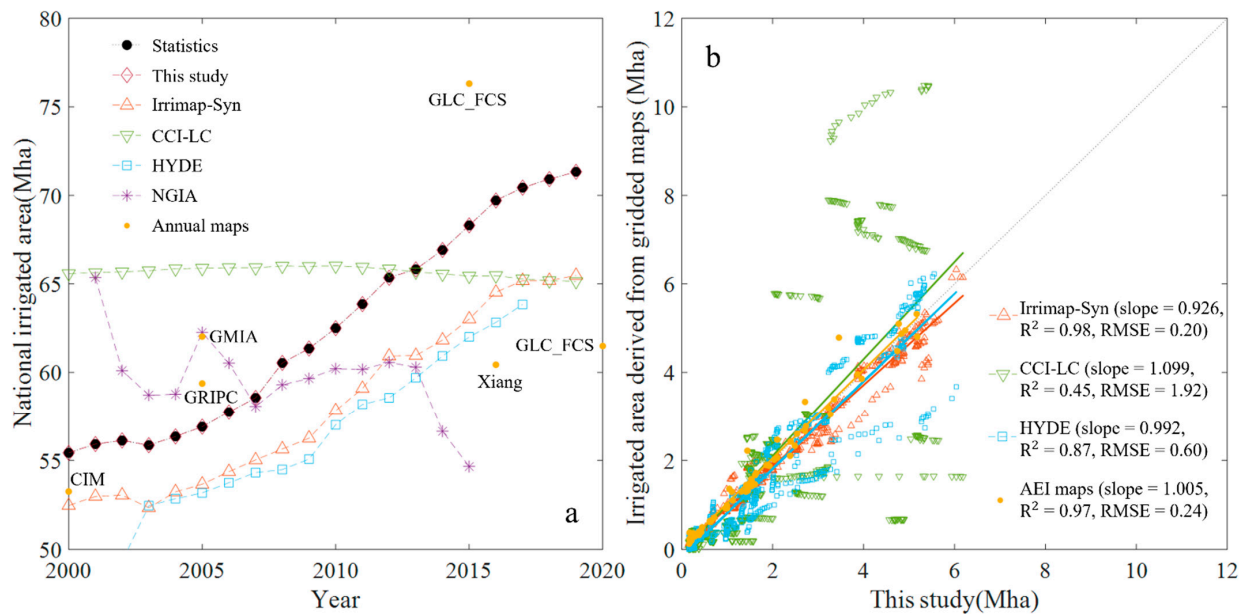


Figure 5. Comparisons among (a) national and (b) provincial irrigated area in China from different gridded datasets. In sub-figure b, the black dash line is the 1:1 line, and colored lines represent linear regression lines (orange: Irrimap-Syn (slope = 0.926, $R^2 = 0.98$, RMSE = 1.92), green: CCI-LC (slope = 1.099, $R^2 = 0.45$, RMSE = 1.92), blue: HYDE (slope = 0.992, $R^2 = 0.87$, RMSE = 0.60), and yellow: AEI maps (slope = 1.005, $R^2 = 0.97$, RMSE = 0.24), which were generated by CIM and GMIA-m to regress with this study).

To present hot spots of irrigation coverage extents and changing trends, we resampled the rebuilt time-series irrigation map and two other datasets (Irrimap-Syn and CCI-LC) from high into coarse spatial resolutions (5 arcmin) and used the annual average irrigation coverage and Sen's slope estimator to compare those three time-series maps with respect to spatial patterns and temporal changes, respectively (Figure 6). Sen's slope estimator, which had strong robustness and error resistance [74], was used to calculate time-series trends in gridded irrigated area. Moreover, the significance of the trend was estimated by the Mann–Kendall significance test [75]. In terms of spatial patterns, the irrigation coverage suggested that both Irrimap-Syn and our rebuilt map shared similarities (Figure 6a,c). It confirmed that the rebuilt irrigation distribution with coarse spatial resolution statistics also retained spatial consistency with Irrimap-Syn dataset with prefecture-level/county-level statistics as input data, and its spatial divergences were mainly reflected in coverage extents as a rebuilt map with higher gridded irrigation coverage in three hot zones, including south Xinjiang Province, Huang-Huai-Hai Plain, and the alluvial plains of Yangtze River Basin. An important reason of these differences was the gap between Irrimap-Syn and statistics (Table A1). In those three hot zones, irrigated areas derived from Irrimap-Syn underestimated about 3.27 Mha in annual average, occupying approximately 70% of the total gap (Table A1). In comparison between CCI-LC and the rebuilt map, divergences were observed in CCI-LC's inadequate coverage of the north and southwest regions, and higher irrigation coverage was observed in Xinjiang, Huai River Basin, and the lower reaches of the Yangtze River Basin (Figure 6a,e). Inadequate coverage led to irrigated area

underestimation. The average underestimated area contributed over 10.68 and 3.21 Mha in northern and southwest provinces, respectively (Table A1). However, total irrigated areas in the provinces of the Huai River Basin and the lower reaches of Yangtze River Basin, including Henan Province, Anhui Province, and Jiangsu Province, etc., were overestimated by about 13.31 Mha in annual average (Table A1). The most overestimated irrigated area was Xinjiang, which had an average of over 6.65 Mha in overestimation, and it is shown as widely high irrigation coverages in Figure 6e.

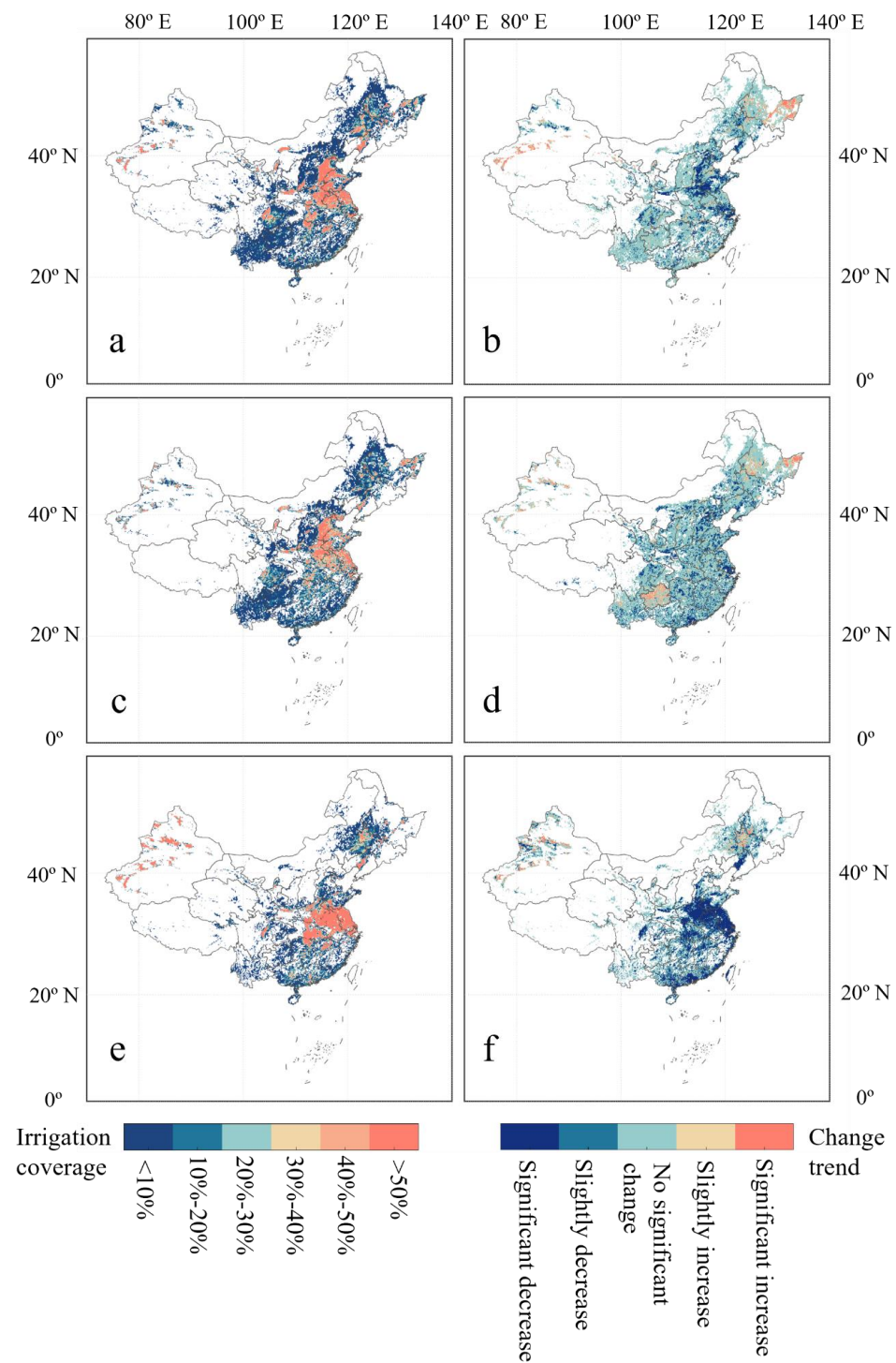


Figure 6. The average coverage (a–e) and change trend (b–f) of irrigated cropland during 2000–2019 in mainland China derived from this study (a,b), Irrimap-Syn (c,d), and CCI-LC (e,f) at 5 arcmin resolution.

In terms of temporal change, Irrimap-Syn and the rebuilt map performed more similarity (Figure 6b,d). Generally, Xinjiang and Heilongjiang showed a significant growth trend, while other hot spots were mainly characterized by a mixture of significant negative growth and non-significant change (Figure 6b,d). In Irrimap-Syn, Guizhou Province and Guangdong Province showed growth in a large spatial extent and decreases at local levels, respectively, due to growth area misestimations (Figure 6d, Table A1). At the center of Huang-Huai-Hai Plain, covering Hebei Province, Shandong Province, and north of Henan Province, irrigated areas had a significant decreasing trend in both the rebuilt and CCI-LC maps, which was different from that in Irrimap-Syn (Figure 6b–f). The area decrease might be caused by water-saving policies in recent years, which required a change from irrigated to rainfed lands in order to relieve serious groundwater depletions [76–80].

3.3. Tracking Irrigated Cropland Changes in China

There were heterogeneous development trends of irrigated cropland in different regions of China, as described in Figure 6. They could be divided into five large areas: Northwest Inland Region (NIR), Northeast Plain (NEP), Huang-Huai-Hai Plain (HHHP, including Haihe River Basin (HARB), the lower reaches of Yellow River Basin, and Huaihe River Basin (HURB)), Yangtze River Basin (YARB), and South China Region (SCR), averaging 14.77%, 14.81%, 34.63%, 24.26%, and 11.53% of the total national irrigated area in two decades, respectively (Figure 7). NIR, covering the Continental Basin (CNB) and middle and upper reaches of the Yellow River Basin (YERB), contributed 3 Mha irrigated area growth in last 20 years, leading to its share increase from 13.33% to 15.17% (Figure 7). The largest area growth occurred in NEP, which increased by over 5.39 Mha in total over two decades, almost by a 5% share increase (Figure 7). In NEP, Heilongjiang Province contributed around three-quarters to growth. The expansion of rice cultivation was the most obvious change resulting from an increase in irrigated area [61,81]. As the most important grain-producing areas in China, HHHP and YARB held the highest irrigation coverage (Figure 6a). Although each achieved an area increase of over 2 Mha, their combined share fell from 62.49% to 56.23% (Figure 7). SCR, covering the Southeast Basin (SEB), Pearl River Basin (PRB), and Southwest Basin (SWB), contributed the smallest area increase (1.60 Mha) and maintained its share at around 11.5% in a 20-year period.

To further obtain the change rule, we summarized irrigated cropland on time information, including start year, end year, and duration period, as described in Figure 8. As a traditional grain-producing zone, HHHP contributed to around half of the total national cereal production [27,82,83]. Its agricultural development was inseparable from irrigation system supports [84]. To increase food production without expanding cropland, the cropping system changed from single to a wheat-maize double cropping rotation with increased irrigation since 1980s [85–87]. As illustrated in Figure 8, it not only held the largest range of irrigated cropland but also maintained it for a long period of time, which helped sustain crop yields and resilience to climate risks but nevertheless led to serious groundwater depletions [77]. Therefore, the expansion of irrigated cropland has gradually slowed (Figure 8c).

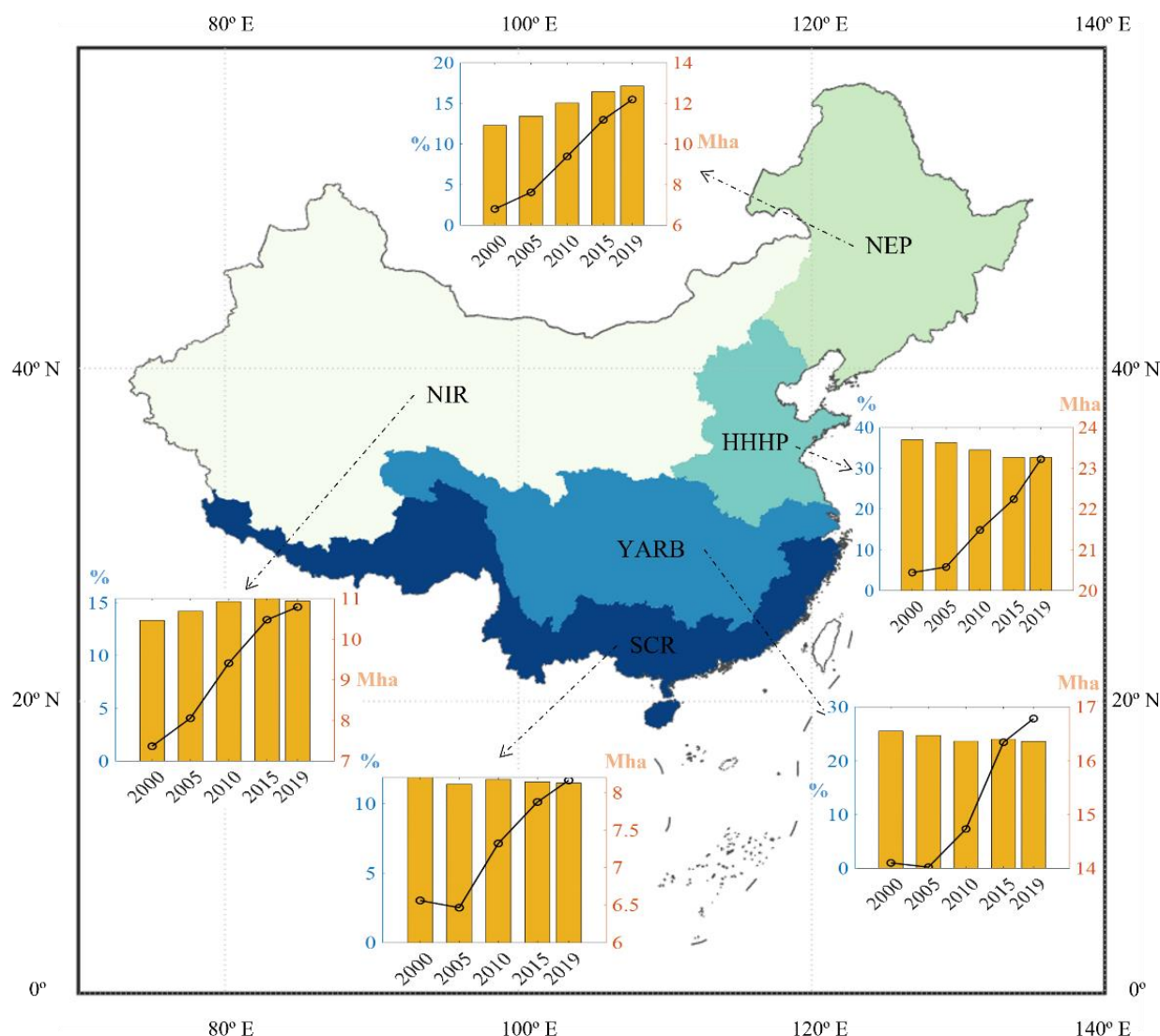


Figure 7. Changes in regional irrigated areas and their proportion from 2000 to 2019.

YARB and SCR were early to realize the development of irrigated agriculture (Figure 8a). Due to the limitation of hilly terrain, their irrigated cropland was mainly distributed in alluvial plains, such as Chengdu Plain, Lianghu Plain, Poyang plain, Yangtze River Delta, and Pearl River Delta. It was found that the irrigation expansion was relatively stable in those irrigated agricultural areas (Figure 8c). Likely due to the rapid urban development in recent years, both withdrawals of irrigated cropland showed a slight increasing trend (Figure 8c). As emerging irrigated agricultural areas, both NIR and NEP started with a low proportion of irrigated cropland but presented different expansion paths (Figure 8c). The Irrigation expansion in NIR slowed down by years, and this specifically manifested as the proportion of new cultivated lands that decreased, while the irrigated cropland in NEP experienced an explosive growth in several years around 2010 (Figure 8c). New irrigated croplands were mainly distributed in Xinjiang Province and Heilongjiang Province, with around 2.15 Mha and 4.15 Mha increases in 20 years, respectively (Figure 8a and Table A1). Their irrigation expansion promoted the increase in cotton and paddy rice planting areas, respectively [61,81,88–90].

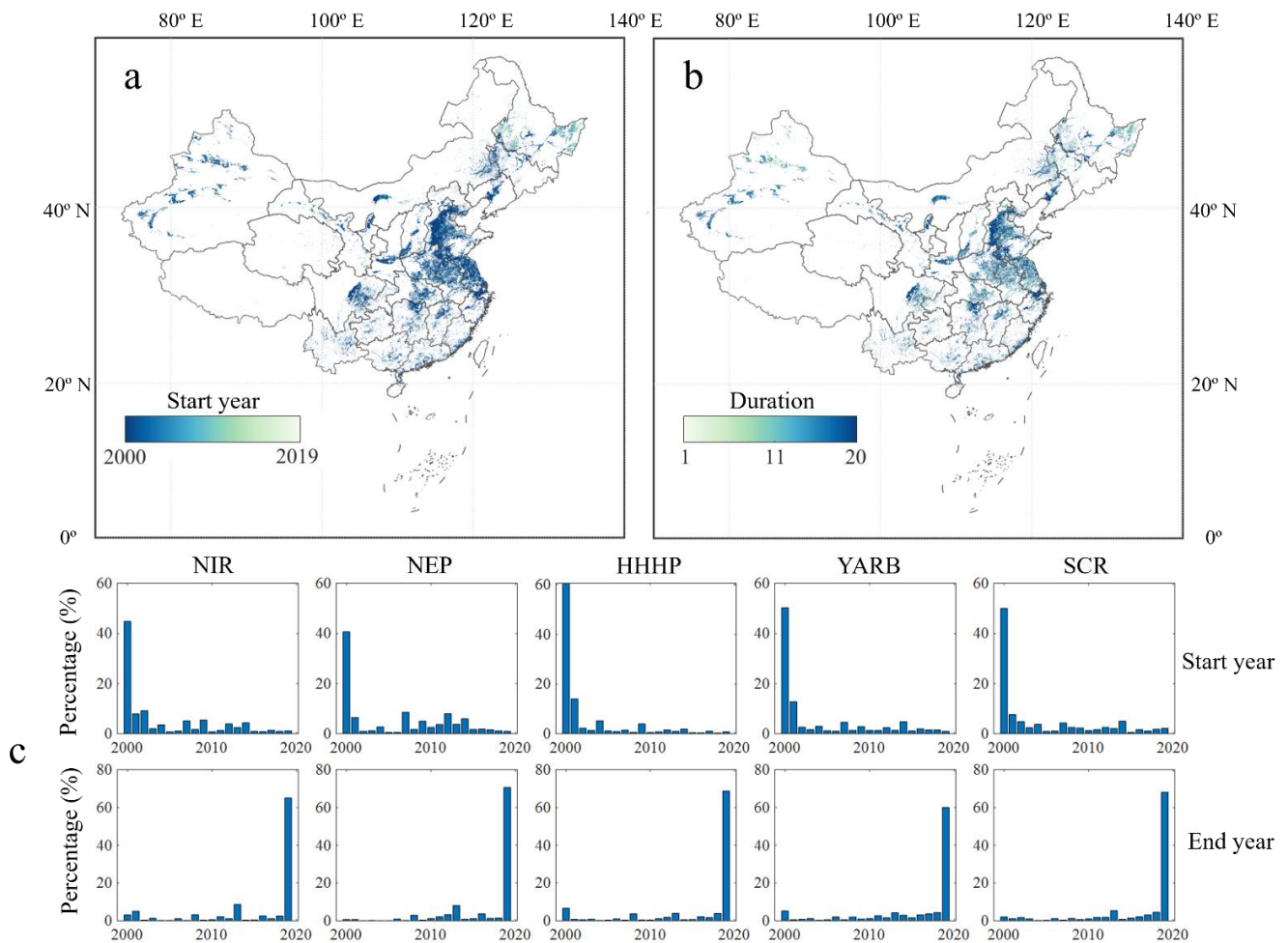


Figure 8. The summary of irrigated cropland changes on time information in China during 2000–2019: (a) the start year distribution of irrigated cropland at 30 arcsec resolution, (b) period duration distribution of irrigated cropland at 30 arcsec resolution, and (c) start and end years' proportion in five large regions.

Both the expansion and abandonment of agricultural irrigation profoundly changed the land-use pattern, as illustrated in Figure 9 and summarized in Table 5 in terms of area gains and losses. In the last 20 years, rainfed cropland was the dominant source of irrigated cropland expansion, followed by pastures, contributing to over 70% and 20% of total area gains, as described in Table 5. The results illustrated that one purpose of large-scale irrigation system constructions in China might be to enhance the intensification of existing agricultural land, since the establishment of irrigated cropping system normally led to high inputs, such as modern varieties, pesticides, and fertilizers, as well as advanced management, such as the conservation of soil and water conservation [1]. Moreover, agricultural land-use intensification was necessary because yield increases were important methods for meeting rapidly increasing demands with limited arable land in China. The irrigated rainfed land-use transition occurred in traditional grain-producing areas, including HHP and the alluvial plains in YERB and YARB, as well as new irrigated areas such as Heilongjiang and Xinjiang (Figure 9b–h). However, for CNB and SCR two regions, other land uses, including woodland, built-up, and others, also provided considerable irrigated area gains (Table 5). In CNB, expansion occurred not only in existing rainfed cropland and pasture but also in unmanaged grazing land (Table 5, Figure 9b–h). These land-use transitions indicated agriculture production from crop-livestock systems changed into intensified cropping systems, which could lift arid climate constraints on agricultural development, thus improving agricultural productivity and local livelihood in CNB. The

hilly terrain shaped the scarcity of land resources in SCR, which was further strained by the Grain for Green policy and urbanization. Therefore, maintaining irrigated agricultural development required the full use of a wider range of land-use transitions (Table 5).

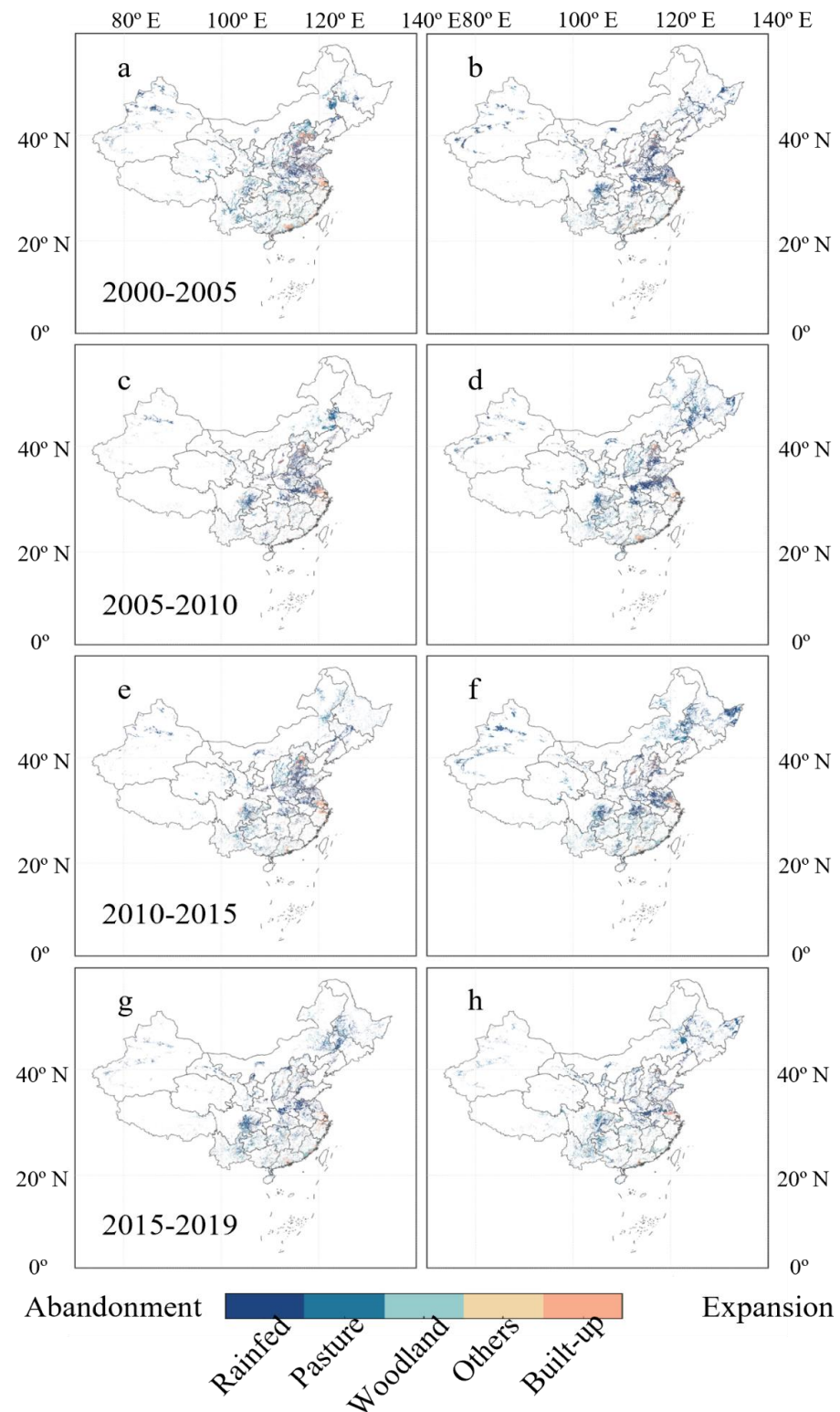


Figure 9. Spatial distributions of land-use transitions caused by irrigated cropland changes during 2000–2019: land-use transitions led by irrigated cropland abandonment (a–g) and expansion (b–h) in 5-year periods.

Table 5. Land-use transition patterns caused by irrigated cropland changes in China during 2000–2019.

		Total Area		Rain Land (%)		Pasture (%)		Woodland (%)		Built-Up (%)		Others (%)	
		Gain	Loss	Gain	Loss	Gain	Loss	Gain	Loss	Gain	Loss	Gain	Loss
NIR	CNB	4.19	1.54	60	74	16	21	0	0	1	4	23	1
	YERB	1.44	0.65	70	60	18	27	0	3	9	10	2	0
	Total	5.63	2.19	62	70	17	23	0	1	3	6	18	1
NEP	\	6.19	0.79	85	71	12	23	1	1	2	6	1	0
HHHP	HARB	2.51	2.37	87	65	3	13	0	2	8	20	1	0
	YERB	0.24	0.46	89	74	5	12	0	1	6	14	0	0
	HURB	5.93	3.06	92	87	2	2	0	0	5	11	0	0
	Total	8.68	5.90	91	77	3	7	0	1	6	15	0	0
YARB	\	7.81	5.12	64	50	21	21	5	8	9	20	1	1
SCR	SEB	0.51	0.34	15	14	17	11	44	25	21	49	2	2
	PRB	2.24	1.26	30	26	35	32	16	22	18	20	1	1
	SWB	0.60	0.14	23	27	43	45	27	19	5	9	2	1
	Total	3.34	1.74	26	23	34	29	22	23	16	25	1	1

Area unit: Mha.

Here, we took rainfed cropping systems with low-level inputs and traditional management as references and investigated irrigation expansions with high-level inputs and advanced management that led to potential positive changes in terms of agricultural drought reduction and soil suitability improvement, as described in Figure 10. Under uneven precipitation distribution, there was a significant spatial difference in the effect of irrigation on water deficit alleviation, a gradual decrease from northwest to southeast, as shown in Figure 10a [27]. The north benefited more from massive irrigation expansions induced by yield constraints that overcame rainfall shortages during cultivation. Hot zones of irrigation expansion in HHHP and NEP were, respectively, in the south and east, which are considerably low water-stress areas at the local level (Figures 9b–h and 10a). It suggested that the irrigation expansion in the north, except NIR, avoided hot spots of water shortage and made a trade-off between water security and food security. During the irrigation expansion process, soil suitability could be widely upgraded into high suitability by improving input and management, especially in key grain-producing areas, such as HHHP, alluvial plains in YARB, Xinjiang in NIR, and Heilongjiang in NEP (Figure 10b). It indicated that irrigation expansion with high inputs and advanced management also could promote crop yield growth by improvements in enhanced soil suitability. Therefore, irrigated cropland expansion in the last two decades could be regarded as an agricultural land-use intensification process, along with the construction of farmland water conservancy infrastructure, production input's increase, and improved management practices.

In terms of irrigated cropland abandonment, irrigated-rainfed land-use transitions contributed to the largest loss (9.59 Mha), about 60% of the total loss during 2000–2019 (Table 5). Moreover, the area loss in developed irrigated areas, HHHP and YARB, was significantly larger than that in NEP and NIR, which are newly developing irrigated regions (Table 4). Thus, such transitions in HHHP and YARB might be related with local water scarcity or land degradation caused by long-term irrigation [77]. As shown in Figure 9, abandonment was mainly distributed in central HHHP and YARB's alluvial plains. Moreover, it might be concerned with unfunctional irrigation due to aging facilities or management neglect [91]. China began renewing supporting facilities and upgrading water-saving facilities in large irrigation districts to improve water-use efficiency and irrigated area recovery [92]. Therefore, after long-term expansions, large-scale irrigated cropland maintenance, water saving, and the conservation of water and soil might be the next priorities.

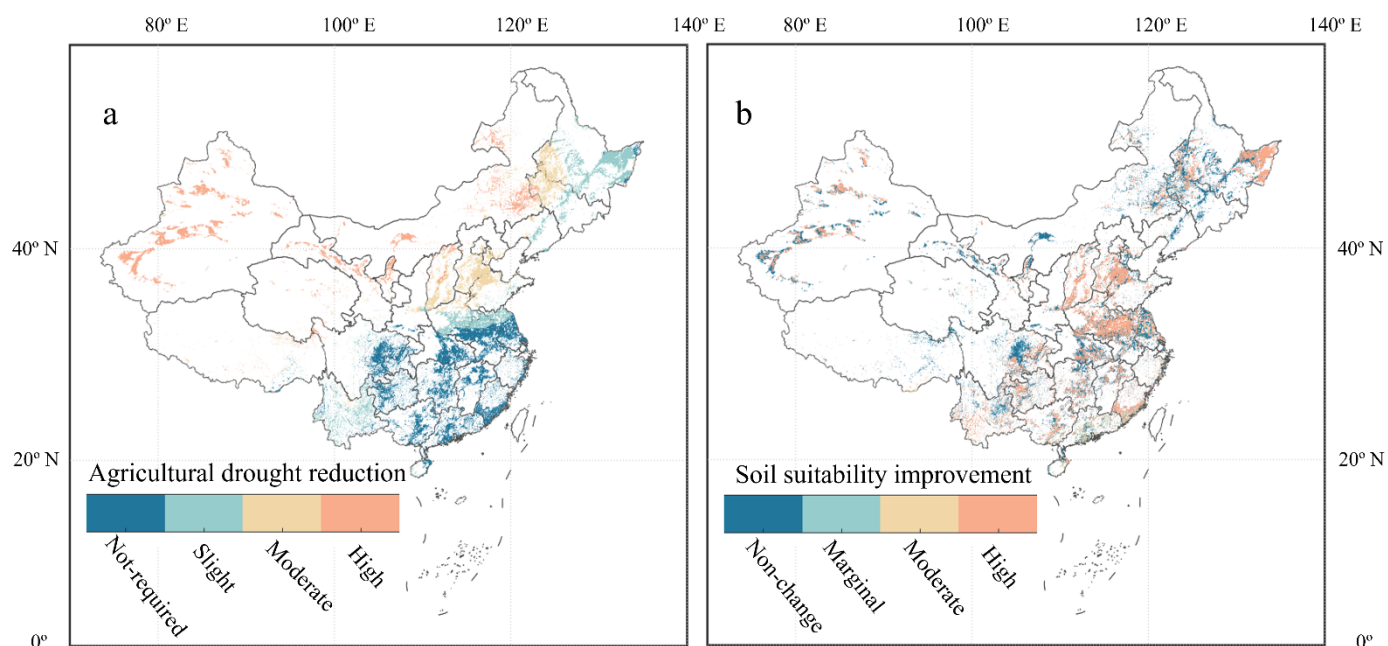


Figure 10. Potential drought reduction (a) and soil suitability improvements (b) caused by irrigated cropland expansion between 2000 and 2019. Calculations can be seen in Appendix A.

As illustrated in Table 5, the Grain for Green policy and urbanization were two other drivers for land abandonment. The Grain for Green policy, as a large-scale political incentive program started in 1999, achieved considerable success in the conservation of water and soil [93–95]. However, the effect on irrigated land outputs was weak, since only unsuitable arable lands, such as sloping, desertification, and heavily polluted land, were involved [96]. As a result, the Grain for Green policy contributed to around 3.55 Mha irrigated area abandonment in the entire period, resulting in cropland–pasture or cropland–woodland transitions (Table 5). YARB and SCR contributed nearly 60% of cropland–pasture and over 90% of cropland–woodland transitions, accounting for two-thirds of total losses from the program (Table 5). Different from the spatial aggregation of other land-use transitions, cropland–pasture and cropland–woodland transitions were scattered in the south between 2000 and 2019 (Figure 9a–g). In the north, the policy effect was pasture or grassland increase due to cropland withdrawals, which was also captured in this study and described in Table 5 [97]. Interestingly, the cropland–pasture transition in NEP and HHHP mainly occurred in the surroundings of irrigated zones, while that in NIR was generally consistent with the expansion distribution (Figure 9), which might be related to the fragile ecological environment caused by severe water stress and soil erosion in the northwest.

The rapid development of industrialization and urbanization in China significantly changed urban–rural land-use patterns and human–land relationships [98], and it caused a direct loss in irrigated land at around 2.52 Mha, occupying about 16% of the total, in the past 20 years (Table 5). Moreover, farmland was indirectly abandoned due to the rural labor shortage from urbanization migration [99]. Compared with marginal land abandonment from the Grain for Green policy, urbanization was more likely to occupy fertile land in the plains, which led to a considerable loss in grain production [99–101]. The rural–urban land-use transition was mainly distributed in the most economically active urban agglomerations of China, including the Jing-Jin-Ji Region, Yangtze River Delta, Pearl River Delta, Weihe (Guanzhong) Plain, central Shanxi Province, northern Henan Province, and the middle reaches of Yangtze River (Figure 9a–g). On the other hand, as a source, it also provided about 2.08 Mha in gains between 2000 and 2019, which reduced the negative impact of urbanization on irrigated agriculture to a certain degree (Table 5). It indicated that Requisition–Compensation Balance of Arable Land policy played a positive role in cropland losses, and the policy required that occupied cropland for non-agricultural use should be

compensated with an equal quality and quantity of arable land within the local scope [98]. Therefore, this form of land replacement was mainly distributed in the surrounding areas of abandoned land from urbanization (Figure 9b–h). For example, abandonment and expansion caused by changes in construction land occurred in the southern and northern areas of Jiangsu, respectively.

4. Discussion

Irrigated agriculture was irreplaceable in terms of food security and resilience against agro-meteorological disasters in China. However, the long-term extensive irrigation led to the overexploitation of water resources. Yet the lack of explicit information on where irrigated land distributed and how irrigated cropland changed throughout time limited trade-off decision making on agricultural sustainable developments in China. Thus, we tracked the dynamics of irrigated cropland in the last two decades by combining multiple data streams (land cover maps, remote-sensing products on irrigation information, and statistics) to reconstruct time-series consistent irrigated cropland maps at 30 arcsec spatial resolution. Our reconstructed map outperformed existing irrigation maps in terms of overall accuracy and consistency with statistics, and the advantage was rebuilt on several factors. At first, a data synergy approach used in the study took full use of multi-sourced heterogeneous datasets to attenuate errors inherited in a single irrigation map [42]. Moreover, the approach can take advantage of complementarities between remote-sensing data and statistics to overcome spatial discrepancies between them [41]. Then, we used more specific observational information on irrigation, such as data on irrigated crops and irrigated cropping system, to reduce uncertainties in traditional irrigation remote-sensing data caused by climate, soil, and crop rotation factors. Finally, considering the influence of drought, rotation, and fallow on the distribution of irrigated cropland, we incorporated a water stress index and previous actual irrigations into the allocation procedure to ensure stability in irrigation distributions over time. To this end, the rebuilt map provided more detailed insights into both the temporal dynamics of irrigated cropland changes and spatial patterns of land-use transitions. Limited by uneven distributions in water and land resources, the expanding land was inevitably concentrated in areas with strained water and land resources [100]. Even so, the expanded irrigation agriculture was far from a mindless unsustainable expansion, because some trade-offs among food security, water security, and land protection were involved in the process, including agricultural land-use intensification, geographical shifts from vulnerable to relatively suitable areas, the Grain for Green policy, and cropland protection in the competition caused by urbanization.

Some limitations and uncertainties cannot be neglected either. First, due to the lack of time-series data, we had to adopt several annual irrigation maps with high spatial resolutions and filled them into neighboring years. However, their spatial discrepancies led to fluctuations in accuracy and distribution at a temporal level and the subsequent overestimation of irrigated land change. There might be two feasible solutions possible in future studies to overcome such fluctuations caused by temporal discontinuity. One method is based on remote-sensing methods to produce time-series data on the actual irrigation in order to replace these annual irrigation maps. The other is to build a dynamic and region-specific score table to reduce uncertainty from local inconsistencies among different inputs [53]. Second, since fragmented lands in China were observed particularly in the south, the spatial resolution of cropland datasets used in this study, which was more suitable for large fields, might limit irrigated cropland mapping [52]. Thus, we guessed that a higher spatial resolution of cropland distribution would be more appropriate, at least in the southern region. Third, although we used provincial-level statistics to achieve higher accuracy and to retain consistency in the spatial pattern with the Irrimap-Syn product, which used prefecture-level/county-level statistics, it was still believed that statistics for smaller administrative geospatial units had an advantage in constraining irrigated cropland extents. The premise of its advantage was built on more detailed data processing and calibration since there were frequent administrative boundary changes and missing

data for a specific year. At last, given the continuous expansion of irrigated cropland, fixed validation samples used in this study might lead to an uncertainty in accuracy assessment, especially in newly irrigated areas and later periods. A more reliable method in future studies would be to collect validation samples for different years to adapt to different development stages.

5. Conclusions

Information on irrigated cropland distribution was critical for agricultural production monitoring, water and land management, and climate change adaptation in China. In this study, we reconstruct irrigated cropland extents across mainland China, covering the period of 2000–2019, by integrating existing irrigation maps, remote-sensing products on irrigated cropping system, and statistics. Moreover, rebuilt maps and other two time-series datasets (CCI-LC and Irrimap-Syn) were validated by using 614 reference samples across mainland China. As a result, our resultant map showed a higher overall accuracy in both average and single years, and it was more consistent with statistics in the terms of the magnitude and overall trend. Moreover, our maps shared a similar spatial pattern with Irrimap-Syn maps, which is different from remote-sensing-based maps (CCI-LC), but there was a slight difference in the temporal change trend, and this was probably because of differences in statistical inputs.

Our resultant maps showed that irrigated areas in China had grown tremendously around 16 Mha over the past two decades but had different growth trends in different regions. As traditional irrigation zones, HHHP and YARB represented simultaneous large-scale expansion and abandonment at the same time, leading to the largest area gains and losses. While in NIR and NEP, which are newly irrigated regions, expansion dominated their dynamics with respect to irrigated cropland, contributing the two largest net area gains. On the temporal scale, their expansion mainly occurred in early and middle periods. In terms of land-use transitions, rainfed cropland was the dominant source of irrigated cropland expansion, followed by pastures, which contributed to over 70% and 20% in total area gains, respectively. As a special case, SCR, constrained by land scarcity, had to make full use of all sources to maintain irrigated agricultural developments. Moreover, the land-use shift from rainfed to the irrigated system resulted in two potential positive changes, water scarcity alleviation and soil suitability improvement, with the indication that agricultural land-use intensification was enhanced by irrigated cropland expansion. Moreover, some efforts on sustainable agriculture development also had been detected, such as geographical shifts from vulnerable to relatively suitable areas, the Grain for Green policy, and cropland protection in the competition of urbanization. Thus, the subsequent consequences of changes in irrigated cropland related to food security and water consumption need further assessments. The reconstructions in this study provide explicit and reliable information on irrigated cropland distributions for applications in agricultural production monitoring, water and land management, and climate change adaptation. Future studies will integrate remote-sensing methods and apply cropland distribution and the statistics of irrigated area with higher spatial resolutions in order to improve classification accuracies. Another possibility is to explore the impact of actual irrigation on crop yields and watershed water resources based on irrigated cropland maps.

Author Contributions: M.B. conducted the research and wrote the manuscript. S.Z. contributed the research design and reviewed the manuscript. T.T. contributed reviewed and edited the manuscript. All authors have read and agreed to the published version of the manuscript.

Funding: This research was sponsored by the National Key Research and Development Program (Grant No. 2019YFC0409000) and approved by the Ministry of Science and Technology of China. And this research was supported by the PKU-IIASA Postdoctoral Program.

Data Availability Statement: Irrigated cropland distribution data in China from 2000 to 2019 presented in this study are available upon request from the corresponding author.

Acknowledgments: We thank Xiufang Zhu from Beijing Normal University for providing a 1 km irrigated area map in China (CIM) and validation samples. We thank J. Meghan Salmon-Tumas from Northland College for providing the Global Rain-Fed, Irrigated, and Paddy Croplands (GRIPC) dataset.

Conflicts of Interest: The authors declare no conflict of interest.

Appendix A

Irrigated cropland expansion may not only reduce drought impacts but also improve soil suitability through increased inputs and strengthen management [1,6–10]. Thus, we used agricultural drought and soil suitability indices to reflect potential gains caused by irrigated cropland expansion. Impacts on drought reduction were calculated by the difference between irrigated and rainfed *WS*. Rainfed *WS* was calculated by Equation (2), ranging from 0 to 1. Irrigated *WS* was set by a fix value (0.8), which was a standard indicating that water requirements for crops were met. Therefore, the impact on drought reduction (*DR*) could be obtained as Equation (A1) shows:

$$DR = \begin{cases} high, & DWS \geq 0.4 \\ moderate, & DWS \geq 0.2 \\ slight, & 0 < DWS < 0.2 \\ not - required, & DWS \leq 0 \end{cases} \quad (A1)$$

where *DR* is divided into four levels, high, moderate, slight, and not-required, according to *DWS*, which denotes the difference between irrigated and rainfed *WS*.

Soil suitability also is also changed by assuming a transition from rainfed cropland or pasture with low input and traditional management to irrigated land with high input and advanced management. Thus, we used the difference in soil suitability between high inputs and low inputs to determine improvements after the expansion. Soil suitability improvement was obtained as follows:

$$SSI = CS \times SSH, \quad (A2)$$

and

$$CS = \begin{cases} 1, & SSH > SSL \\ 0, & SSH \leq SSL \end{cases} \quad (A3)$$

where *SSI* represents soil suitability improvements after the expansion, which is obtained by a changing state and soil suitability with high inputs; *CS* denotes a state variable that is 1 if soil suitability with high inputs (*SSH*) is greater than that with low inputs (*SSL*) and 0 otherwise. Moreover, both soil suitability indices with high inputs and low inputs were obtained from the GAEZv4 dataset [70]. *SSI* is divided into four levels, including non-change, marginal, moderate, and high. Non-change represents no improvements after the expansion, while the other three levels correspond to a soil suitability index with high inputs (high level: very high and high; moderate level: medium and moderate; and marginal level: marginal and very marginal).

Appendix B

Table A1. Area differences with statistics in average and irrigated area changes of Irrimap-Syn, CCI-LC, and HYDE at a provincial level from 2000 to 2019.

Province Name	Statistics		Irrimap-Syn		CCI-LC		HYDE	
	Average Area	Area Changes	Area Differences with Statistics	Area Changes	Area Differences with Statistics	Area Changes	Area Differences with Statistics	Area Changes
Beijing	247	−225	191	−238	−170	−1	63	35
Tianjin	359	−62	352	−25	−233	−1	92	73
Hebei	4753	−39	4300	−160	−3627	−19	−90	647

Table A1. Cont.

Province Name	Statistics		Irrimap-Syn		CCI-LC		HYDE	
	Average Area	Area Changes	Area Differences with Statistics	Area Changes	Area Differences with Statistics	Area Changes	Area Differences with Statistics	Area Changes
Shanxi	1309	454	1185	314	−993	−6	−58	362
Nei Mongol	2893	830	2577	449	−849	212	−1306	533
Liaoning	1629	205	1525	230	−265	−65	−384	947
Jilin	1675	607	1669	589	339	159	−242	1759
Heilongjiang	3937	4151	3892	4236	−2268	36	−1841	2673
Shanghai	234	−95	208	−95	186	−94	41	12
Jiangsu	3989	368	4055	266	3220	−412	749	126
Zhejiang	1490	28	1368	−44	379	−221	−115	437
Anhui	3786	1405	3647	1374	4182	−151	427	416
Fujian	1045	204	908	28	−398	−73	−630	340
Jiangxi	1961	171	1892	137	463	−55	237	305
Shandong	5288	469	4791	484	−2282	−118	555	874
Henan	5076	614	4922	669	1968	−273	485	560
Hubei	2487	937	2199	350	3541	−106	276	589
Hunan	2892	516	2819	410	211	−73	−92	62
Guangdong	1804	400	1835	−193	624	−192	−453	639
Guangxi	1599	266	1514	3	638	−90	−177	761
Hainan	238	126	177	21	11	−18	−81	177
Chongqing	664	73	626	211	−443	−24	122	591
Sichuan	2682	608	2428	581	−1179	−82	−98	1165
Guizhou	928	506	1128	965	−752	−16	−509	498
Yunnan	1666	563	1556	377	−839	−29	−922	588
Xizang	222	138	123	−41	39	9	−200	39
Shaanxi	1393	11	1247	125	−83	−43	−118	249
Gansu	1209	377	1046	163	−392	45	−494	616
Qinghai	211	5	169	−20	1	8	−123	95
Ningxia Hui	490	150	447	49	−150	3	−170	130
Xinjiang Uygur	4337	2151	3352	1797	6657	1251	−1740	1258
Sum	62,494	15,912	58,151	13,010	7537	−439	−6797	17,553

Area unit: Mha.

References

1. Yu, Q.; You, L.; Wood-Sichra, U.; Ru, Y.; Joglekar, A.K.B.; Fritz, S.; Xiong, W.; Lu, M.; Wu, W.; Yang, P. A cultivated planet in 2010—Part 2: The global gridded agricultural-production maps. *Earth Syst. Sci. Data* **2020**, *12*, 3545–3572. [\[CrossRef\]](#)
2. Godfray, H.C.J.; Beddington, J.R.; Crute, I.R.; Haddad, L.; Lawrence, D.; Muir, J.F.; Pretty, J.; Robinson, S.; Thomas, S.M.; Toulmin, C. Food Security: The Challenge of Feeding 9 Billion People. *Science* **2010**, *327*, 812–818. [\[CrossRef\]](#)
3. Gibbs, H.K.; Ruesch, A.S.; Achard, F.; Clayton, M.K.; Holmgren, P.; Ramankutty, N.; Foley, J.A. Tropical forests were the primary sources of new agricultural land in the 1980s and 1990s. *Proc. Natl. Acad. Sci. USA* **2010**, *107*, 16732–16737. [\[CrossRef\]](#)
4. Foley, J.A.; Defries, R.; Asner, G.P.; Barford, C.; Bonan, G.; Carpenter, S.R.; Chapin, F.S.; Coe, M.T.; Daily, G.C.; Gibbs, H.K.; et al. Global consequences of land use. *Science* **2005**, *309*, 570–574. [\[CrossRef\]](#)
5. Ramankutty, N.; Evan, A.T.; Monfreda, C.; Foley, J.A. Farming the planet: 1. Geographic distribution of global agricultural lands in the year 2000. *Glob. Biogeochem. Cycles* **2008**, *22*. [\[CrossRef\]](#)
6. Mueller, N.D.; Gerber, J.S.; Johnston, M.; Ray, D.K.; Ramankutty, N.; Foley, J.A. Closing yield gaps through nutrient and water management. *Nature* **2012**, *490*, 254–257. [\[CrossRef\]](#)
7. Rosa, L.; Rulli, M.C.; Davis, K.F.; Chiarelli, D.D.; Passera, C.; D’Odorico, P. Closing the yield gap while ensuring water sustainability. *Environ. Res. Lett.* **2018**, *13*, 104002. [\[CrossRef\]](#)
8. Brown, J.F.; Pervez, M.S. Merging remote sensing data and national agricultural statistics to model change in irrigated agriculture. *Agric. Syst.* **2014**, *127*, 28–40. [\[CrossRef\]](#)
9. Zhang, J.; Guan, K.; Peng, B.; Pan, M.; Zhou, W.; Jiang, C.; Kimm, H.; Franz, T.E.; Grant, R.F.; Yang, Y.; et al. Sustainable irrigation based on co-regulation of soil water supply and atmospheric evaporative demand. *Nat. Commun.* **2021**, *12*, 5549. [\[CrossRef\]](#)
10. Wang, X.; Muller, C.; Elliot, J.; Mueller, N.D.; Ciais, P.; Jagermeyr, J.; Gerber, J.; Dumas, P.; Wang, C.; Yang, H.; et al. Global irrigation contribution to wheat and maize yield. *Nat. Commun.* **2021**, *12*, 1235. [\[CrossRef\]](#)
11. Wada, Y.; van Beek, L.P.H.; van Kempen, C.M.; Reckman, J.W.T.M.; Vasak, S.; Bierkens, M.F.P. Global depletion of groundwater resources. *Geophys. Res. Lett.* **2010**, *37*, 1–5. [\[CrossRef\]](#)

12. Droppers, B.; Supit, I.; van Vliet, M.T.H.; Ludwig, F. Worldwide water constraints on attainable irrigated production for major crops. *Environ. Res. Lett.* **2021**, *16*, 055016. [[CrossRef](#)]
13. Siebert, S.; Döll, P. Quantifying blue and green virtual water contents in global crop production as well as potential production losses without irrigation. *J. Hydrol.* **2010**, *384*, 198–217. [[CrossRef](#)]
14. Huang, Q.; Rozelle, S.; Lohmar, B.; Huang, J.; Wang, J. Irrigation, agricultural performance and poverty reduction in China. *Food Policy* **2006**, *31*, 30–52. [[CrossRef](#)]
15. Döll, P.; Müller Schmied, H.; Schuh, C.; Portmann, F.T.; Eicker, A. Global-scale assessment of groundwater depletion and related groundwater abstractions: Combining hydrological modeling with information from well observations and GRACE satellites. *Water Resour. Res.* **2014**, *50*, 5698–5720. [[CrossRef](#)]
16. Shiklomanov, I.A. Appraisal and Assessment of World Water Resources. *Water Int.* **2000**, *25*, 11–32. [[CrossRef](#)]
17. Döll, P.; Siebert, S. Global modeling of irrigation water requirements. *Water Resour. Res.* **2002**, *38*, 8-1–8-10. [[CrossRef](#)]
18. Scanlon, B.R.; Jolly, I.; Sophocleous, M.; Zhang, L. Global impacts of conversions from natural to agricultural ecosystems on water resources: Quantity versus quality. *Water Resour. Res.* **2007**, *43*, 215–222. [[CrossRef](#)]
19. Meier, J.; Zabel, F.; Mauser, W. A global approach to estimate irrigated areas—A comparison between different data and statistics. *Hydrol. Earth Syst. Sci.* **2018**, *22*, 1119–1133. [[CrossRef](#)]
20. Huang, Q.; Wang, J.; Li, Y. Do water saving technologies save water? Empirical evidence from North China. *J. Environ. Econ. Manag.* **2017**, *82*, 1–16. [[CrossRef](#)]
21. Tilman, D.; Balzer, C.; Hill, J.; Befort, B.L. Global food demand and the sustainable intensification of agriculture. *Proc. Natl. Acad. Sci. USA* **2011**, *108*, 20260–20264. [[CrossRef](#)]
22. Foley, J.A.; Ramankutty, N.; Brauman, K.A.; Cassidy, E.S.; Gerber, J.S.; Johnston, M.; Mueller, N.D.; O’Connell, C.; Ray, D.K.; West, P.C.; et al. Solutions for a cultivated planet. *Nature* **2011**, *478*, 337–342. [[CrossRef](#)]
23. Grafton, R.Q.; Williams, J.; Jiang, Q. Possible pathways and tensions in the food and water nexus. *Earth’s Future* **2017**, *5*, 449–462. [[CrossRef](#)]
24. Nagaraj, D.; Proust, E.; Todeschini, A.; Rulli, M.C.; D’Odorico, P. A new dataset of global irrigation areas from 2001 to 2015. *Adv. Water Resour.* **2021**, *152*, 103910. [[CrossRef](#)]
25. Dinar, A.; Tieu, A.; Huynh, H. Water scarcity impacts on global food production. *Glob. Food Secur.* **2019**, *23*, 212–226. [[CrossRef](#)]
26. Han, Z. Strategy on high quality development of large and medium irrigation districts in the new period. *China Water Resour.* **2021**, *17*, 15–17+14. [[CrossRef](#)]
27. Piao, S.; Ciais, P.; Huang, Y.; Shen, Z.; Peng, S.; Li, J.; Zhou, L.; Liu, H.; Ma, Y.; Ding, Y.; et al. The impacts of climate change on water resources and agriculture in China. *Nature* **2010**, *467*, 43–51. [[CrossRef](#)]
28. Fischer, G.; Chen, Y.; Sun, L. *The Balance of Cultivated Land in China during 1988–1995*; International Institute for Applied Systems Analysis: Laxenburg, Austria, 1998.
29. Wu, P.; Jin, J.; Zhao, X. Impact of climate change and irrigation technology advancement on agricultural water use in China. *Clim. Change* **2010**, *100*, 797–805. [[CrossRef](#)]
30. Varis, O.; Vakkilainen, P. China’s 8 challenges to water resources management in the first quarter of the 21st Century. *Geomorphology* **2001**, *41*, 93–104. [[CrossRef](#)]
31. Molle, F.; Mollinga, P.P.; Wester, P. Hydraulic Bureaucracies and the Hydraulic Mission: Flows of water, Flows of power. *Water Altern.* **2009**, *2*, 328–349.
32. Zhu, X.; Zhu, W.; Zhang, J.; Pan, Y. Mapping Irrigated Areas in China From Remote Sensing and Statistical Data. *IEEE J. Sel. Top. Appl. Earth Obs. Remote Sens.* **2014**, *7*, 4490–4504. [[CrossRef](#)]
33. Liu, J.; Zang, C.; Tian, S.; Liu, J.; Yang, H.; Jia, S.; You, L.; Liu, B.; Zhang, M. Water conservancy projects in China: Achievements, challenges and way forward. *Glob. Environ. Chang.* **2013**, *23*, 633–643. [[CrossRef](#)]
34. Pervez, M.S.; Brown, J.F. Mapping Irrigated Lands at 250-m Scale by Merging MODIS Data and National Agricultural Statistics. *Remote Sens.* **2010**, *2*, 2388–2412. [[CrossRef](#)]
35. Ozdogan, M.; Yang, Y.; Allez, G.; Cervantes, C. Remote Sensing of Irrigated Agriculture: Opportunities and Challenges. *Remote Sens.* **2010**, *2*, 2274–2304. [[CrossRef](#)]
36. Zhang, C.; Dong, J.; Zuo, L.; Ge, Q. Tracking spatiotemporal dynamics of irrigated croplands in China from 2000 to 2019 through the synergy of remote sensing, statistics, and historical irrigation datasets. *Agric. Water Manag.* **2022**, *263*, 107458. [[CrossRef](#)]
37. Xie, Y.; Lark, T.J.; Brown, J.F.; Gibbs, H.K. Mapping irrigated cropland extent across the conterminous United States at 30 m resolution using a semi-automatic training approach on Google Earth Engine. *ISPRS J. Photogramm. Remote Sens.* **2019**, *155*, 136–149. [[CrossRef](#)]
38. Liang, S.; Wang, J. (Eds.) Remote sensing application in agriculture. In *Advanced Remote Sensing*, 2nd ed.; Academic Press: Cambridge, MA, USA, 2020; Chapter 24; pp. 871–914. [[CrossRef](#)]
39. Yang, H.; Zhang, X.; Zehnder, A.J.B. Water scarcity, pricing mechanism and institutional reform in northern China irrigated agriculture. *Agric. Water Manag.* **2003**, *61*, 143–161. [[CrossRef](#)]
40. Ambika, A.K.; Wardlow, B.; Mishra, V. Remotely sensed high resolution irrigated area mapping in India for 2000 to 2015. *Sci. Data* **2016**, *3*, 160118. [[CrossRef](#)]
41. Lu, M.; Wu, W.; You, L.; See, L.; Fritz, S.; Yu, Q.; Wei, Y.; Chen, D.; Yang, P.; Xue, B. A cultivated planet in 2010—Part 1: The global synergy cropland map. *Earth Syst. Sci. Data* **2020**, *12*, 1913–1928. [[CrossRef](#)]

42. Winkler, K.; Fuchs, R.; Rounsevell, M.; Herold, M. Global land use changes are four times greater than previously estimated. *Nat. Commun.* **2021**, *12*, 2501. [CrossRef]
43. Frolking, S.; Qiu, J.; Boles, S.; Xiao, X.; Liu, J.; Zhuang, Y.; Li, C.; Qin, X. Combining remote sensing and ground census data to develop new maps of the distribution of rice agriculture in China. *Glob. Biogeochem. Cycles* **2002**, *16*, 38–1–38–10. [CrossRef]
44. Salmon, J.M.; Friedl, M.A.; Frolking, S.; Wisser, D.; Douglas, E.M. Global rain-fed, irrigated, and paddy croplands: A new high resolution map derived from remote sensing, crop inventories and climate data. *Int. J. Appl. Earth Obs. Geoinf.* **2015**, *38*, 321–334. [CrossRef]
45. Thenkabail, P.; Teluguntla, P.; Xiong, J.; Oliphant, A.; Massey, R. *NASA MEaSUREs Global Food Security Support Analysis Data (GFSAD) Crop Mask 2010 Global 1 km V001*; NASA EOSDIS Land Processes DAAC: Sioux Falls, SD, USA, 2016. [CrossRef]
46. Xiang, K.; Yuan, W.; Wang, L.; Deng, Y. An LSWI-Based Method for Mapping Irrigated Areas in China Using Moderate-Resolution Satellite Data. *Remote Sens.* **2020**, *12*, 4181. [CrossRef]
47. ESA. *Land Cover CCI Product User Guide Version 2*; ESA: Paris, France, 2017.
48. Klein Goldewijk, K.; Beusen, A.; Doelman, J.; Stehfest, E. Anthropogenic land use estimates for the Holocene—HYDE 3.2. *Earth Syst. Sci. Data* **2017**, *9*, 927–953. [CrossRef]
49. Deines, J.M.; Kendall, A.D.; Crowley, M.A.; Rapp, J.; Cardille, J.A.; Hyndman, D.W. Mapping three decades of annual irrigation across the US High Plains Aquifer using Landsat and Google Earth Engine. *Remote Sens. Environ.* **2019**, *233*, 111400. [CrossRef]
50. Xu, T.; Deines, J.; Kendall, A.; Basso, B.; Hyndman, D. Addressing Challenges for Mapping Irrigated Fields in Subhumid Temperate Regions by Integrating Remote Sensing and Hydroclimatic Data. *Remote Sens.* **2019**, *11*, 370. [CrossRef]
51. Frolking, S.; Xiao, X.; Zhuang, Y.; Salas, W.; Li, C. Agricultural land-use in China a comparison of area estimates from ground-based census and satellite-borne remote sensing. *Glob. Ecol. Biogeogr.* **1999**, *8*, 407–416. [CrossRef]
52. Fritz, S.; See, L.; McCallum, I.; You, L.; Bun, A.; Moltchanova, E.; Duerauer, M.; Albrecht, F.; Schill, C.; Perger, C.; et al. Mapping global cropland and field size. *Glob. Chang. Biol.* **2015**, *21*, 1980–1992. [CrossRef]
53. Lu, M.; Wu, W.; You, L.; Chen, D.; Zhang, L.; Yang, P.; Tang, H. A Synergy Cropland of China by Fusing Multiple Existing Maps and Statistics. *Sensors* **2017**, *17*, 1613. [CrossRef]
54. Siebert, S.; Kumm, M.; Porkka, M.; Döll, P.; Ramankutty, N.; Scanlon, B.R. A global data set of the extent of irrigated land from 1900 to 2005. *Hydrol. Earth Syst. Sci.* **2015**, *19*, 1521–1545. [CrossRef]
55. U.S. Department of Agriculture. *Summary Report: 2007 National Resources Inventory*; Natural Resources Conservation Service: Washington, DC, USA; Center for Survey Statistics and Methodology, I.S.U.: Ames, IA, USA, 2009.
56. Winkler, K.; Fuchs, R.; Rounsevell, M.D.A.; Herold, M. *HILDA+ Global Land Use Change between 1960 and 2019*; PANGAEA: Minneapolis, MN, USA, 2020. [CrossRef]
57. Liu, J.; Kuang, W.; Zhang, Z.; Xu, X.; Qin, Y.; Ning, J.; Zhou, W.; Zhang, S.; Li, R.; Yan, C.; et al. Spatiotemporal characteristics, patterns, and causes of land-use changes in China since the late 1980s. *J. Geogr. Sci.* **2014**, *24*, 195–210. [CrossRef]
58. Zhang, X.; Liu, L.; Chen, X.; Gao, Y.; Xie, S.; Mi, J. GLC_FCS30: Global land-cover product with fine classification system at 30 m using time-series Landsat imagery. *Earth Syst. Sci. Data* **2021**, *13*, 2753–2776. [CrossRef]
59. Siddiqui, S.; Cai, X.; Chandrasekharan, K. *Irrigated Area Map Asia and Africa*; International Water Management Institute (IWMI): Colombo, Sri Lanka, 2016.
60. Luo, Y.; Zhang, Z.; Chen, Y.; Li, Z.; Tao, F. ChinaCropPhen1km: A high-resolution crop phenological dataset for three staple crops in China during 2000–2015 based on leaf area index (LAI) products. *Earth Syst. Sci. Data* **2020**, *12*, 197–214. [CrossRef]
61. Zhang, G.; Xiao, X.; Biradar, C.M.; Dong, J.; Qin, Y.; Menarguez, M.A.; Zhou, Y.; Zhang, Y.; Jin, C.; Wang, J.; et al. Spatiotemporal patterns of paddy rice croplands in China and India from 2000 to 2015. *Sci. Total Environ.* **2017**, *579*, 82–92. [CrossRef]
62. Han, J.; Zhang, Z.; Luo, Y.; Cao, J.; Zhang, L.; Cheng, F.; Zhuang, H.; Zhang, J. *APRA500: A 500 m Annual Paddy Rice Dataset for Monsoon Asia Using Multisource Remote Sensing Data*; Zenodo: Geneva, Switzerland, 2021. [CrossRef]
63. Han, J.; Zhang, Z.; Luo, Y.; Cao, J.; Zhang, L.; Zhuang, H.; Cheng, F.; Zhang, J.; Tao, F. Annual paddy rice planting area and cropping intensity datasets and their dynamics in the Asian monsoon region from 2000 to 2020. *Agric. Syst.* **2022**, *200*, 103437. [CrossRef]
64. China Irrigation and Drainage Development Center. *Water-Saving Efficient Irrigation System for Wheat. A Series of Lectures on Water-Saving and Efficient Irrigation System for Major Crops in China*. 2008. Available online: http://www.jsjg.com.cn/CIDD_C_SavingWaterClass_3/Index2_1.htm#2.1 (accessed on 30 June 2022).
65. Luo, Y.; Zhang, Z.; Li, Z.; Chen, Y.; Zhang, L.; Cao, J.; Tao, F. *Data for: Identifying the Spatiotemporal Changes of Annual Harvesting Areas for Three Staple Crops in China by Integrating Multi-Data Sources*, 2nd ed.; Mendeley Data: New York, NY, USA, 2020. [CrossRef]
66. Luo, Y.; Zhang, Z.; Li, Z.; Chen, Y.; Zhang, L.; Cao, J.; Tao, F. Identifying the spatiotemporal changes of annual harvesting areas for three staple crops in China by integrating multi-data sources. *Environ. Res. Lett.* **2020**, *15*, 074003. [CrossRef]
67. Liu, L.; Xu, X.; Zhuang, D.; Chen, X.; Li, S. Changes in the potential multiple cropping system in response to climate change in China from 1960–2010. *PLoS ONE* **2013**, *8*, e80990. [CrossRef]
68. Monfreda, C.; Ramankutty, N.; Foley, J.A. Farming the planet: 2. Geographic distribution of crop areas, yields, physiological types, and net primary production in the year 2000. *Glob. Biogeochem. Cycles* **2008**, *22*. [CrossRef]
69. Han, J.; Zhang, Z.; Luo, Y.; Cao, J.; Zhang, L.; Cheng, F.; Zhuang, H.; Zhang, J. *ACIA500: A 500 m Annual Cropping Intensity Dataset for Monsoon Asia Based on MODIS Data*; Zenodo: Geneva, Switzerland, 2021. [CrossRef]

70. FAO; IIASA. Global Agro Ecological Zones Version 4 (GAEZv4). Available online: <http://www.fao.org/gaez/> (accessed on 20 January 2022).
71. Trambauer, P.; Maskey, S.; Werner, M.; Pappenberger, F.; van Beek, L.P.H.; Uhlenbrook, S. Identification and simulation of space–time variability of past hydrological drought events in the Limpopo River basin, southern Africa. *Hydrol. Earth Syst. Sci.* **2014**, *18*, 2925–2942. [[CrossRef](#)]
72. Wambura, F.J. Sensitivity of the Evapotranspiration Deficit Index to Its Parameters and Different Temporal Scales. *Hydrology* **2021**, *8*, 26. [[CrossRef](#)]
73. Wu, W.-b.; Yang, P.; Tang, H.-j.; Zhou, Q.-b.; Chen, Z.-x.; Shibasaki, R. Characterizing Spatial Patterns of Phenology in Cropland of China Based on Remotely Sensed Data. *Agric. Sci. China* **2010**, *9*, 101–112. [[CrossRef](#)]
74. Sen, P.K. Estimates of the Regression Coefficient Based on Kendall’s Tau. *J. Am. Stat. Assoc.* **1968**, *63*, 1379–1389. [[CrossRef](#)]
75. Kossack, C.F.; Kendall, M.G. Rank correlation methods. *Am. Math. Mon.* **1950**, *57*, 425–426. [[CrossRef](#)]
76. Wang, J.; Li, Y.; Huang, J.; Yan, T.; Sun, T. Growing water scarcity, food security and government responses in China. *Glob. Food Secur.* **2017**, *14*, 9–17. [[CrossRef](#)]
77. Xu, Z.; Chen, X.; Liu, J.; Zhang, Y.; Chau, S.; Bhattarai, N.; Wang, Y.; Li, Y.; Connor, T.; Li, Y. Impacts of irrigated agriculture on food-energy-water-CO₂ nexus across metacoupled systems. *Nat. Commun.* **2020**, *11*, 5837. [[CrossRef](#)]
78. *General Plan for the Development of Water-Saving Reduction-Mining and High-Efficiency Water-Saving Irrigation in North China (2014–2018)*; China Irrigation and Drainage Development Center: Beijing, China, 2014; Available online: <http://www.jsgg.com.cn/Index/Display.asp?NewsID=20209> (accessed on 30 June 2022).
79. Action Plan for Comprehensive Control of Groundwater Overexploitation in North China. C.M.o.W. Resources. 2019. Available online: http://szy.mwr.gov.cn/zcfg/fg/202008/t20200819_1433310.html (accessed on 30 June 2022).
80. The Ministry of Water Resources of the National Development and Reform Commission. National Action Plan for Water Conservation. 2019. Available online: http://www.gov.cn/gongbao/content/2019/content_5419221.htm (accessed on 30 June 2022).
81. Xin, F.; Xiao, X.; Dong, J.; Zhang, G.; Zhang, Y.; Wu, X.; Li, X.; Zou, Z.; Ma, J.; Du, G.; et al. Large increases of paddy rice area, gross primary production, and grain production in Northeast China during 2000–2017. *Sci. Total Environ.* **2020**, *711*, 135183. [[CrossRef](#)]
82. Liu, Y.; Wang, E.; Yang, X.; Wang, J. Contributions of climatic and crop varietal changes to crop production in the North China Plain, since 1980s. *Glob. Chang. Biol.* **2010**, *16*, 2287–2299. [[CrossRef](#)]
83. Liu, Y.; Long, H.; Li, T.; Tu, S. Land use transitions and their effects on water environment in Huang-Huai-Hai Plain, China. *Land Use Policy* **2015**, *47*, 293–301. [[CrossRef](#)]
84. Yu, Z.; Jin, X.; Miao, L.; Yang, X. A historical reconstruction of cropland in China from 1900 to 2016. *Earth Syst. Sci. Data* **2021**, *13*, 3203–3218. [[CrossRef](#)]
85. Jeong, S.-J.; Ho, C.-H.; Piao, S.; Kim, J.; Ciaia, P.; Lee, Y.-B.; Jhun, J.-G.; Park, S.K. Effects of double cropping on summer climate of the North China Plain and neighbouring regions. *Nat. Clim. Chang.* **2014**, *4*, 615–619. [[CrossRef](#)]
86. Meng, Q.; Sun, Q.; Chen, X.; Cui, Z.; Yue, S.; Zhang, F.; Römheld, V. Alternative cropping systems for sustainable water and nitrogen use in the North China Plain. *Agric. Ecosyst. Environ.* **2012**, *146*, 93–102. [[CrossRef](#)]
87. Wang, J.; Zhang, Y.; Gong, S.; Xu, D.; Juan, S.; Zhao, Y. Evapotranspiration, crop coefficient and yield for drip-irrigated winter wheat with straw mulching in North China Plain. *Field Crops Res.* **2018**, *217*, 218–228. [[CrossRef](#)]
88. Feike, T.; Khor, L.Y.; Mamitim, Y.; Ha, N.; Li, L.; Abdusalih, N.; Xiao, H.; Doluschitz, R. Determinants of cotton farmers’ irrigation water management in arid Northwestern China. *Agric. Water Manag.* **2017**, *187*, 1–10. [[CrossRef](#)]
89. Li, S. (Ed.) *Agricultural Statistics of China (1949–2019)*; Rural Social and Economic Survey Division, National Bureau of Statistics: Beijing, China, 2020.
90. Zhang, T.; Zhai, Y.; Ma, X.; Shen, X.; Bai, Y.; Zhang, R.; Ji, C.; Hong, J. Towards environmental sustainability: Life cycle assessment-based water footprint analysis on China’s cotton production. *J. Clean. Prod.* **2021**, *313*, 127925. [[CrossRef](#)]
91. A Brief Introduction to the Planning for the Extension of Supporting Facilities and Water-Saving Transformation in Large Irrigation Areas of China. 2003. Available online: <http://www.jsgg.com.cn/Index/Display.asp?NewsID=1735> (accessed on 1 July 2022).
92. Chen, M. Accelerating modernization of irrigation district for high quality development. *China Water Resour.* **2021**, *17*, 1–3. [[CrossRef](#)]
93. Chen, Y.; Wang, K.; Lin, Y.; Shi, W.; Song, Y.; He, X. Balancing green and grain trade. *Nat. Geosci.* **2015**, *8*, 739–741. [[CrossRef](#)]
94. Chen, C.; Park, T.; Wang, X.; Piao, S.; Xu, B.; Chaturvedi, R.K.; Fuchs, R.; Brovkin, V.; Ciaia, P.; Fensholt, R.; et al. China and India lead in greening of the world through land-use management. *Nat. Sustain.* **2019**, *2*, 122–129. [[CrossRef](#)]
95. Bryan, B.A.; Gao, L.; Ye, Y.; Sun, X.; Connor, J.D.; Crossman, N.D.; Stafford-Smith, M.; Wu, J.; He, C.; Yu, D.; et al. China’s response to a national land-system sustainability emergency. *Nature* **2018**, *559*, 193–204. [[CrossRef](#)]
96. Suggestions on Strengthening the Protection of Cultivated Land and Improving Requisition–Compensation Balance. Available online: http://www.gov.cn/zhengce/2017-01/23/content_5162649.htm (accessed on 22 July 2022).
97. Huang, L.; Xiao, T.; Zhao, Z.; Sun, C.; Liu, J.; Shao, Q.; Fan, J.; Wang, J. Effects of grassland restoration programs on ecosystems in arid and semiarid China. *J. Environ. Manag.* **2013**, *117*, 268–275. [[CrossRef](#)]
98. Liu, Y.; Fang, F.; Li, Y. Key issues of land use in China and implications for policy making. *Land Use Policy* **2014**, *40*, 6–12. [[CrossRef](#)]

99. Li, T.; Long, H.; Zhang, Y.; Tu, S.; Ge, D.; Li, Y.; Hu, B. Analysis of the spatial mismatch of grain production and farmland resources in China based on the potential crop rotation system. *Land Use Policy* **2017**, *60*, 26–36. [[CrossRef](#)]
100. Zuo, L.; Zhang, Z.; Carlson, K.M.; MacDonald, G.K.; Brauman, K.A.; Liu, Y.; Zhang, W.; Zhang, H.; Wu, W.; Zhao, X.; et al. Progress towards sustainable intensification in China challenged by land-use change. *Nat. Sustain.* **2018**, *1*, 304–313. [[CrossRef](#)]
101. He, C.; Liu, Z.; Xu, M.; Ma, Q.; Dou, Y. Urban expansion brought stress to food security in China: Evidence from decreased cropland net primary productivity. *Sci. Total Environ.* **2017**, *576*, 660–670. [[CrossRef](#)] [[PubMed](#)]